Diffusion Monte Carlo methods for spin-orbit-coupled ultracold Bose gases

J. Sánchez-Baena,* J. Boronat,† and F. Mazzanti‡

Departament de Física, Universitat Politècnica de Catalunya, Campus Nord B4-B5, E-08034 Barcelona, Spain

We present two diffusion Monte Carlo (DMC) algorithms for systems of ultracold quantum gases featuring synthetic spin-orbit interactions. The first one is a spin-integrated DMC method which provides fixed-phase energy estimates. The second one is a discrete spin generalisation of the T-moves spin-orbit DMC [Melton *et al.*, J. Chem. Phys. **144**, 244113 (2016)], which provides an upper bound to the fixed-phase energy. The former is a more accurate method but it is restricted to spin-independent two-body interactions. We report a comparison between both algorithms for different systems. As a check of the efficiency of both methods, we compare the DMC energies with results obtained with other numerical methods, finding agreement between both estimations.

I. INTRODUCTION

The interplay between the electron spin and its momentum, known as spin-orbit coupling (SOC), is an effect of major relevance when studying a wide variety of systems in the field of solid-state physics, such as Majorana fermions [1], spintronic devices [2] or topological insulators [3]. The realization in the last few years of a synthetic SOC interaction in ultracold atomic gases, by exploiting the space-dependent coupling of the atoms with a properly designed configuration of laser beams [4–7], represents an important achievement. More interestingly, these new realizations allow for a better understanding of the effects induced by the SOC interaction, since ultracold quantum gases are highly controllable and tunable [8]. Ultracold SOC quantum gases have been studied in the dilute regime [9], showing the rise of new exotic phases, such as a spin-polarized plane wave phase and a stripe phase. This stripe phase has been recently observed by Li *et al.* [10] showing specific properties of a supersolid phase.

Up to now, the theoretical approaches used in the study of SOC gases rely on the mean-field approximation. This theory is expected to be valid when the gas parameter is very small, $na^3 \leqslant 10^{-5}$, but beyond this limit one is faced with beyond-mean field terms. A way of surpassing the range of applicability of the mean-field approximation is the use of quantum Monte Carlo (QMC) methods, which are not based on any perturbative scheme. In the present work, we use QMC to study these ultracold atomic gases featuring a synthetic SOC interaction. In particular, we work with the diffusion Monte Carlo (DMC) method, which is a stochastic method intended for solving the imaginary-time many-body Schrödinger equation. The action of the imaginary-time propagator $\exp[-\tau \hat{H}]$ is implemented as a set of transformations to a list of points in coordinate space (commonly called *walkers*) that represent statistically the wave function. In the limit $\tau \to \infty$, the ground state dominates while excited-state contributions are

exponentially damped, providing an exact estimate of the ground-state energy and of any observable commuting with $\hat{H}$. If the ground state of the system of interest is complex (which is the case when the SOC term is present), it is necessary to invoke the fixed-phase approximation (FPA) [11], which provides an upper bound to the ground-state energy.

Previous DMC calculations with SOC terms in the Hamiltonian have been carried out in the study of electronic structures [11,12], quantum dots in semiconductors [13], and repulsive Fermi gases [14]. A DMC method incorporating the SOC terms that arise in electronic systems has already been developed [11]. In this method, the authors implement the spin-orbit term of the propagator through the use of the T-moves technique [15]. They also use a regularized, continuous representation of the spin degrees of freedom. In order to control the sign problem that the SOC terms introduce in the propagator, the authors of Ref. [11] define an effective Hamiltonian in such a way that the propagator becomes positive-definite. It can be shown that the estimations obtained with this effective Hamiltonian yield an upper bound to the fixed-phase energy [16]. In the present paper, we adapt the T-moves DMC algorithm of Ref. [11] to the usual, discrete representation of the spin, and show how to treat the synthetic SOC present in ultracold quantum gases. We also introduce a different method for treating the SOC terms of the propagator, loosely based on Ref. [17], which consists on propagating the wave function integrated over all spin configurations. In doing so, we avoid almost completely the sign problem induced by SOC terms, meaning that no effective Hamiltonian needs to be defined.

This paper is organized as follows. In Sec. II we discuss the form of the Hamiltonian as well as several kinds of spin-orbit couplings of interest in the field of cold Bose gases. The reduced units used in this work are introduced in Sec. II A. In Sec. III we present the details concerning the spin-integrated DMC. We derive the algorithm starting from the spin-orbit propagator in the FPA and present a scheme to clarify how to implement it. In Sec. IV we show how to implement discrete spin sampling within the T-moves DMC, as well as how to implement the SOC terms introduced in Sec. II. In Sec. V we compare both DMC methods in one and two-body problems (Sec. V A) and in some many-body cases (Sec. V B).

*juan.sanchez.baena@upc.edu
†jordi.boronat@upc.edu
‡ferran.mazzanti@upc.edu

Finally, in Sec. VI we summarize the main conclusions of our work.

II. HAMILTONIAN

The system studied in this work is formed by an ultracold gas of N bosons of mass M with pseudo-spin $1/2$ under the effect of synthetic spin-orbit coupling [8]. The generic form of the Hamiltonian is

$$\hat{H} = \sum_{k=1}^{N} \left[\frac{\hat{P}_k^2}{2M} + \hat{V}_k^{1b} + \hat{W}_k^{SOC} \right] + \hat{V}^{2b} \qquad (1)$$

with $\hat{V}_k^{1b}$ and $\hat{V}^{2b}$ momentum independent, local, one- and two-body interactions, respectively. Notice that $\hat{V}^{2b}$ can depend on the spin configuration. In much the same way, $\hat{W}_k^{SOC}$ stands for a one-body, momentum, and spin-dependent potential. The ones considered in this work are the Rashba, Weyl, and Raman interactions given by

$$\hat{W}_k^{Rs} = \frac{\lambda_{Rs}\hbar}{2} \left[\hat{P}_k^y \hat{\sigma}_k^x - \hat{P}_k^x \hat{\sigma}_k^y \right], \qquad (2)$$

$$\hat{W}_k^{Rm} = \frac{\lambda_{Rm}\hbar}{M} \hat{P}_k^x \hat{\sigma}_k^z + \frac{\lambda_{Rm}^2 \hbar^2}{2M} - \frac{\Omega}{2} \hat{\sigma}_k^x, \qquad (3)$$

$$\hat{W}_k^{We} = \frac{\lambda_{We}\hbar}{M} \left[\hat{P}_k^x \hat{\sigma}_k^x + \hat{P}_k^y \hat{\sigma}_k^y + \hat{P}_k^z \hat{\sigma}_k^z \right] + \frac{\lambda_{We}^2 \hbar^2}{2M}, \qquad (4)$$

with $\hat{P}_k^\alpha$ the α component of the momentum operator of particle k, $\hat{\sigma}_k^{x,y,z}$ the Pauli matrices associated to particle k, Ω the Rabi frequency, and λ_α ($\alpha = \{ Rs, We, Rm \}$) the strength of the corresponding SOC interaction. The general form of the two-body potential is

$$\hat{V}^{2b} = \sum_{k<l} \left[\sum_{s_k, s_l} V_{s_k, s_l}^{2b}(r_{kl}) |s_k, s_l\rangle \langle s_k, s_l| \right], \qquad (5)$$

where s_k, s_l assign values ± 1 to the z component of the spin of particles k and l, while $V_{s_k, s_l}^{2b}(r_{kl})$ is a central, short-ranged potential that can be different for the different channels corresponding to s_k and s_l. In the numerical examples of Sec. V we use a soft-core force, defined by

$$V_{s_k, s_l}(r) = V_0(s_k, s_l)\theta[R_0(s_k, s_l) - r]. \qquad (6)$$

If the two-body interaction is taken to be spin-independent, $V_0(s_k, s_l) = V_0$ and $R_0(s_k, s_l) = R_0$.

The one-body potential used in some of the calculations below is

$$\hat{V}^{1b} = \tfrac{1}{2} M\omega^2 (\hat{X}^2 + \hat{Y}^2 + \hat{Z}^2). \qquad (7)$$

A. Reduced units for the different kinds of SOC interactions

Due to the different spin dependence, we use different length and energy scales in each case. These are the following: for the Rashba interaction, we set the length and energy units to

$$a_{Rs} = \frac{1}{\lambda_{Rs}M}, \quad e_{Rs} = \frac{\hbar^2}{2Ma_{Rs}^2} = \frac{\hbar^2 \lambda_{Rs}^2 M}{2}, \qquad (8)$$

while for the Raman interaction

$$a_{Rm} = \frac{\eta_{Rm}}{\lambda_{Rm}}, \quad e_{Rm} = \frac{\hbar^2}{2Ma_{Rm}^2} = \frac{\hbar^2 \lambda_{Rm}^2}{2M\eta_{Rm}^2} \qquad (9)$$

with η_{Rm} a dimensionless scaling factor that we vary depending on the density. Finally, for the Weyl Hamiltonian we use

$$a_{We} = \frac{\eta_{We}}{2\lambda_{We}}, \quad e_{We} = \frac{\hbar^2}{2Ma_{We}^2} = \frac{2\hbar^2 \lambda_{We}^2}{M\eta_{We}^2}. \qquad (10)$$

In terms of these, the interactions read

$$\hat{W}_k^{Rashba} = \left[\hat{P}_k^y \hat{\sigma}_k^x - \hat{P}_k^x \hat{\sigma}_k^y \right], \qquad (11)$$

$$\hat{W}_k^{Raman} = 2\eta_{Rm} \hat{P}_k^x \hat{\sigma}_k^z + \eta_{Rm}^2 - \frac{\Omega}{2} \hat{\sigma}_k^x, \qquad (12)$$

$$\hat{W}_k^{Weyl} = \eta_{We} \left[\hat{P}_k^x \hat{\sigma}_k^x + \hat{P}_k^y \hat{\sigma}_k^y + \hat{P}_k^z \hat{\sigma}_k^z \right] + \frac{\eta_{We}^2}{4}, \qquad (13)$$

where all quantities are dimensionless. The same applies to the soft-core potential and harmonic trap of Eqs. (6) and (7).

III. THE SPIN-INTEGRATED DMC (SIDMC) METHOD

In this section, we derive the spin-integrated DMC algorithm (SIDMC). This is done starting from the propagator in the FPA, and writing the imaginary time evolution equation for the spin-integrated probability density. In the following, we assume the two-body interaction is spin-independent. We also present a scheme of the SIDMC algorithm and address some relevant technical details.

A. Formalism

The FPA propagator up to $O(\Delta\tau)$ is given by (see Appendix A)

$$G_{FP}(\vec{R}, \vec{S} \to \vec{R}', \vec{S}')$$
$$= \langle \vec{R}', \vec{S}' | \exp[-\Delta\tau \hat{H}^{FP}] | \vec{R}, \vec{S} \rangle$$
$$\simeq \int d\vec{R}'' \langle \vec{R}', \vec{S}' | \exp[-\Delta\tau (\hat{w}_{Re} + \hat{V}_\Phi)] | \vec{R}'', \vec{S} \rangle$$
$$\times \langle \vec{R}'' | \exp[-\Delta\tau \hat{H}_0] | \vec{R} \rangle, \qquad (14)$$

with

$$\hat{H}_0 = \sum_{k=1}^{N} \left[\frac{P_k^2}{2M} + \hat{V}_k^{1b} + \sum_{l<k}^{N} \hat{V}_{k,l}^{2b} \right], \qquad (15)$$

$$\hat{W} = \sum_{k=1}^{N} \hat{W}_k^{SOC}, \qquad (16)$$

$$\langle \vec{R}, \vec{S} | \hat{w}_{Re} | \vec{R}', \vec{S}' \rangle = \operatorname{Re} \left\{ \langle \vec{R}, \vec{S} | \hat{W} | \vec{R}', \vec{S}' \rangle \frac{e^{i\Phi(\vec{R}', \vec{S}')}}{e^{i\Phi(\vec{R}, \vec{S})}} \right\}, \qquad (17)$$

$$\langle \vec{R}', \vec{S}' | \hat{V}_\Phi | \vec{R}, \vec{S} \rangle = \left[\sum_{k=1}^{N} |\boldsymbol{\nabla}_k \Phi(\vec{R}, \vec{S})|^2 \right]$$
$$\times \delta(\vec{R}' - \vec{R})\delta(\vec{S}' - \vec{S}), \qquad (18)$$

$$\hat{H}^{FP} = \hat{H}_0 + \hat{w}_{Re} + \hat{V}_\Phi, \qquad (19)$$

and $\Phi(\vec{R}, \vec{S})$ is the phase fixed by the FPA. In this approximation one has to impose a certain form for the phase. In this

work we impose it to be the sum of one-body terms

$$\Phi(\vec{R}, \vec{S}) = \sum_{k=1}^{N} \phi_k(\vec{r}_k, s_k). \tag{20}$$

Due to the form of the spin-orbit potential, we can evaluate the integral in Eq. (14). For the Raman SOC of Eq. (3), the matrix element of the spin-dependent part of the potential is

$$\langle \vec{R}', \vec{S}' | \hat{w}_{\text{Re}} + \hat{V}_\Phi | \vec{R}'', \vec{S} \rangle = \sum_{k=1}^{N} \left[\prod_{l \neq k}^{N} \delta_{\vec{r}_l', \vec{r}_l''} \delta_{s_l', s_l} \right] \left[\frac{\lambda \hbar}{M} \delta_{y_k', y_k''} \delta_{z_k', z_k''} \frac{d\delta_{x_k', x_k''}}{dx_k'} \langle s_k' | \hat{\sigma}_k^z | s_k \rangle \sin(\Delta\phi_k) + \frac{\lambda^2}{2M} \delta_{\vec{r}_k', \vec{r}_k''} \delta_{s_k', s_k} \right.$$
$$\left. + |\vec{\nabla}_k \phi_k|^2 \delta_{\vec{r}_k', \vec{r}_k''} \delta_{s_k', s_k} - \frac{\Omega}{2} \langle s_k' | \hat{\sigma}_k^x | s_k \rangle \cos(\Delta\phi_k) \delta_{\vec{r}_k', \vec{r}_k''} \right], \tag{21}$$

where

$$\Delta\phi_k = \phi_k(\vec{r}_k'', s_k) - \phi_k(\vec{r}_k', s_k'). \tag{22}$$

Since the spinless part of the propagator is given by Ref. [18], one has

$$\langle \vec{R}'' | \exp[-\Delta\tau \hat{H}_0] | \vec{R} \rangle = \exp\left[-\frac{M}{2\hbar^2 \Delta\tau} (\vec{R}'' - \vec{R})^2 \right] \exp\left\{ \Delta\tau \left[E_s - \frac{V_0(\vec{R}'') + V_0(\vec{R}'')}{2} \right] \right\}, \tag{23}$$

with V_0 the spinless part of the potential entering in $\hat{H}_0$ and E_s the common energy shift used in the DMC algorithm. Up to $O(\Delta\tau)$, the integral in Eq. (14) yields

$$G_{\text{FP}}(\vec{R}, \vec{S} \rightarrow \vec{R}', \vec{S}') = \langle \vec{R}' | \exp[-\Delta\tau \hat{H}_0] | \vec{R} \rangle \left\{ \delta_{\vec{S}', \vec{S}} - \Delta\tau \sum_{k=1}^{N} \left[\prod_{l \neq k}^{N} \delta_{s_l', s_l} \right] \left[\frac{\lambda \hbar}{M} \langle s_k' | \hat{\sigma}_k^z | s_k \rangle \cos(\Delta\phi_k) \right. \right.$$
$$\left. \left. \times \frac{\partial \phi_k}{\partial x_k''} + \frac{\lambda^2}{2M} \delta_{s_k', s_k} - \frac{\Omega}{2} \langle s_k' | \hat{\sigma}_k^x | s_k \rangle \cos(\Delta\phi_k) + |\vec{\nabla}_k \phi_k|^2 \delta_{s_k', s_k} \right] |_{\vec{R}'' = \vec{R}'} \right\}. \tag{24}$$

For the Rashba and Weyl SOC interactions, a similar procedure has to be carried out. However, one has to expand the element $\langle \vec{R}', \vec{S}' | \exp[-\Delta\tau(\hat{w}_{\text{Re}} + \hat{V}_\Phi)] | \vec{R}'', \vec{S} \rangle$ in Eq. (14) up to order $\Delta\tau^2$. This is because the terms originated from the matrix element of $\hat{w}_{\text{Re}}$ are proportional to $\xi_k = r_k' - r_k$, and thus, the elements arising from $\hat{w}_{\text{Re}}^2$ generate contributions of order ξ_k^2 and $\xi_k \xi_l$. Since ξ_k represents the displacement of particle k due to the standard DMC Gauss-drift-branching (GDB) process, this quantity is of $O(\sqrt{\Delta\tau})$. However, in the numerical experiments conducted, we have not found a significant impact on the results when these terms are dropped.

Following with the derivation of the propagator in Eq. (24), we define a new operator $\hat{O}$ as

$$\langle \vec{S}' | \hat{O}(\vec{R}') | \vec{S} \rangle = \frac{G_{\text{FP}}(\vec{R}, \vec{S} \rightarrow \vec{R}', \vec{S}')}{\langle \vec{R}' | \exp[-\Delta\tau \hat{H}_0] | \vec{R} \rangle}, \tag{25}$$

while, up to $O(\Delta\tau)$, Eq. (24) can be rewritten as

$$G_{\text{FP}}(\vec{R}, \vec{S} \rightarrow \vec{R}', \vec{S}') \simeq \langle \vec{R}' | \exp[-\Delta\tau \hat{H}_0] | \vec{R} \rangle \prod_{k=1}^{N} \left\{ \delta_{s_k', s_k} - \Delta\tau \left[\frac{\lambda \hbar}{M} \langle s_k' | \hat{\sigma}_k^z | s_k \rangle \cos(\Delta\phi_k) \right. \right.$$
$$\left. \times \frac{\partial \phi_k}{\partial x_k''} + \frac{\lambda^2}{2M} \delta_{s_k', s_k} - \frac{\Omega}{2} \langle s_k' | \hat{\sigma}_k^x | s_k \rangle \cos(\Delta\phi_k) + |\vec{\nabla}_k \phi_k|^2 \delta_{s_k', s_k} \right] |_{\vec{r}_k'' = \vec{r}_k'} \right\}$$
$$= \langle \vec{R}' | \exp[-\Delta\tau \hat{H}_0] | \vec{R} \rangle \prod_{k=1}^{N} \langle s_k' | \hat{O}_k(\vec{r}_k') | s_k \rangle, \tag{26}$$

where we have used the approximation $(1 - \Delta t \sum x_i) \approx \prod(1 - \Delta t x_i)$ which is exact to order Δt. In this way, the matrix element of the new operator $\hat{O}$ becomes the product of matrix elements of single-particle operators $\hat{O}_k$, as shown in the expression above.

Note that, for the Rashba and Weyl SOCs, the matrix elements $\langle s_k' | \hat{O}_k | s_k \rangle$ depend on both $\vec{r}_k'$ and $\vec{r}_k$. For the sake of simplicity, in the following we omit the r_k and r_k' labels. The imaginary time evolution equation for the magnitude of the wave function, within the FPA and to order Δt, is given by (see Appendix A)

$$\rho(\vec{R}', \vec{S}', \tau + \Delta\tau) = \sum_{\vec{S}} \int d\vec{R} \left\{ \prod_{k=1}^{N} \langle s_k' | \hat{O}_k | s_k \rangle \langle \vec{R}' | \exp[-\Delta\tau \hat{H}_0] | \vec{R} \rangle \rho(\vec{R}, \vec{S}, \tau) \right\}. \tag{27}$$

However, in DMC simulations the object that is propagated is $f(\vec{R}, \vec{S}, \tau) = \rho(\vec{R}, \vec{S}, \tau)\rho_T(\vec{R}, \vec{S})$, with $\rho_T(\vec{R}, \vec{S})$ the magnitude of a given importance sampling trial function. From Eq. (27) one readily sees that

$$f(\vec{R}', \vec{S}', \tau + \Delta\tau) = \sum_{\vec{S}} \int d\vec{R} \left\{ \prod_{k=1}^{N} \langle s_k'|\hat{O}_k|s_k\rangle \langle \vec{R}'| \exp[-\Delta\tau \hat{H}_0]|\vec{R}\rangle \frac{\rho_T(\vec{R}', \vec{S}')}{\rho_T(\vec{R}, \vec{S})} f(\vec{R}, \vec{S}, \tau) \right\}. \tag{28}$$

In order to implement this equation, we need the propagator to be positive-definite. However, due to the spin-orbit coupling, the matrix elements of the propagator do not fulfill this condition. Despite this, if we propagate the spin-integrated form of the magnitude of the importance sampling function f of Eq. (28), this problem is greatly reduced. Therefore, we propagate the quantity

$$F(\vec{R}, \tau) = \sum_{\vec{S}} f(\vec{R}, \vec{S}, \tau). \tag{29}$$

In order to progress, we impose the magnitude of the trial wave function to be spin-independent, i.e., $\rho_T(\vec{R}, \vec{S}) = \rho_T(\vec{R})$. After j time steps, one gets

$$F(\vec{R}^{(j)}, j\Delta\tau) = \sum_{\vec{S}^{(j)},...,\vec{S}^{(0)}} \int d\vec{R}^{(j-1)} \cdots d\vec{R}^{(0)}$$

$$\times \prod_{n=1}^{j} \left(\prod_{k=1}^{N} \langle s_k^{(n)}|\hat{O}_k|s_k^{(n-1)}\rangle \right)$$

$$\times \prod_{n=1}^{j} \langle \vec{R}^{(n)}| \exp[-\Delta\tau \hat{H}_0]|\vec{R}^{(n-1)}\rangle$$

$$\times \frac{\rho_T(\vec{R}^{(n)})}{\rho_T(\vec{R}^{(n-1)})} F(\vec{R}^{(0)}, 0), \tag{30}$$

where $\vec{R}^{(n)}$ are the position coordinates of the walker, and $s_k^{(n)}$ the spin of particle k of that walker, both at iteration n. We can understand this expression in a simple way. The last two pieces correspond to a standard GDB DMC process [18] for the spinless part of the Hamiltonian. On the other hand, the first part, incorporating the spin-dependent terms, can be implemented through a secondary branching process. This one must fulfill that, after j iterations, the weight carried by a given walker is given by

$$w(j) = \sum_{\vec{S}^{(j)},...,\vec{S}^{(0)}} \prod_{n=1}^{j} \left(\prod_{k=1}^{N} \langle s_k^{(n)}|\hat{O}_k|s_k^{(n-1)}\rangle \right), \tag{31}$$

corresponding to the first term in Eq. (30). This is fulfilled by performing the secondary branching at iteration j using the weight

$$B(j) = \frac{w(j)}{w(j-1)} \tag{32}$$

with the initial condition $w(0) = 1$. It can be shown that $w(j)$ can be easily computed as

$$w(j) = \prod_{k=1}^{N} [c_k^+(j) + c_k^-(j)] = \prod_{k=1}^{N} w_k(j), \tag{33}$$

in terms of the spin weight factors

$$\begin{pmatrix} c_k^+(j) \\ c_k^-(j) \end{pmatrix} = \left[\prod_{n=1}^{j} \begin{pmatrix} \langle\uparrow|\hat{O}_k|\uparrow\rangle & \langle\uparrow|\hat{O}_k|\downarrow\rangle \\ \langle\downarrow|\hat{O}_k|\uparrow\rangle & \langle\downarrow|\hat{O}_k|\downarrow\rangle \end{pmatrix} \right] \begin{pmatrix} 1 \\ 1 \end{pmatrix}$$

$$= \begin{pmatrix} \langle\uparrow|\hat{O}_k|\uparrow\rangle & \langle\uparrow|\hat{O}_k|\downarrow\rangle \\ \langle\downarrow|\hat{O}_k|\uparrow\rangle & \langle\downarrow|\hat{O}_k|\downarrow\rangle \end{pmatrix} \begin{pmatrix} c_k^+(j-1) \\ c_k^-(j-1) \end{pmatrix}, \tag{34}$$

where $|\uparrow\rangle$ and $|\downarrow\rangle$ stand for $|s = 1\rangle$ and $|s = -1\rangle$, respectively. In this way, in the proposed method each walker carries the evolution of both c^+ and c^- for every particle, instead of explicit spin variables. Notice that these factors constitute the fundamental quantities that define the secondary branching of Eq. (32). In this way, these factors account for the change in norm of the propagator.

B. The SIDMC algorithm

In this section we present a scheme of the spin-integrated DMC algorithm. In the present method, a walker is represented by the set of quantities

$$\vec{v} = (\vec{r}_1, \ldots, \vec{r}_N, c_1^+, c_1^-, \ldots, c_N^+, c_N^-). \tag{35}$$

Particle positions are initialized as usual in Monte Carlo simulations, while spin weight factors $c_k^\pm$ must be initialized to one in the first iteration

$$c_k^\pm = 1 \, \forall k. \tag{36}$$

The first step in each iteration of the algorithm is to perform a standard GDB process using the spinless part of the Hamiltonian $\hat{H}_0$ and $\rho_T(\vec{R})$. Next, one has to update the $c_k^\pm$ coefficients according to the expression

$$\begin{pmatrix} c_k^+(j+1) \\ c_k^-(j+1) \end{pmatrix} = \boldsymbol{O}_k^{(j+1)} \begin{pmatrix} c_k^+(j) \\ c_k^-(j) \end{pmatrix}, \tag{37}$$

which yields the new coefficients at iteration $j+1$ from the known ones at iteration j. Notice that, in this expression, $\boldsymbol{O}_k$ is the 2×2 matrix of Eq. (34). Once with these coefficients, one can obtain $w(j+1)$ according to

$$w(j+1) = \left\{ \prod_{k=1}^{N} [c_k^+(j+1) + c_k^-(j+1)] \right\}, \tag{38}$$

and from here, the secondary branching factor,

$$B(j+1) = \frac{w(j+1)}{w(j)}. \tag{39}$$

Notice this weight is different for each walker, so in fact $B = B_{i_w}$ with i_w the walker index. Notice that the branching process with total replication factor $B_{\text{tot}}(j+1) = B_{\text{spinless}}(j+1)B(j+1)$ is in this way split in two parts, which are performed one after the other, for convenience.

In practice, it may happen that, along the simulation, the absolute value of the $c_k^{\pm}(j)$ coefficients keeps increasing unboundedly. However, the ratio of w's in this equation is always finite. On the other hand, it is better to use a mixed-branching strategy with the $B(j+1)$ terms, where walkers acquire a weight that is being updated along each block of iterations. The accumulated weight $\mathcal{B}_{i_w}$ at the end of the block is equal to the product of the weights at each iteration, for each walker. Once the block is finished, these weights are used to replicate the list of walkers.

In DMC simulations, the weight of the walkers is divided by a constant (equal to $e^{E_T \Delta\tau}$ with E_T the threshold energy and $\Delta\tau$ the time step) when performing the replication process [18]. One has to perform an equivalent renormalization with the secondary branching, while in this case the normalization constant can be computed in two ways. One way is to use the average over the final number of walkers of the accumulated B of the previous block. Another way is to use the B coefficients of the current block, accumulated over the previous iterations and averaged over the number of walkers. The best strategy is determined by the SOC model at hand, with the first choice being more suitable for the Raman interaction, and the latter performing better with the Weyl and Rashba models.

The energy at iteration i inside a block is estimated as (see Appendix B)

$$E_{DMC}^{(i)} = \frac{\sum_{i_w=1}^{N_w} E_{i_w}^{(i)} \mathcal{B}_{i_w}}{\sum_{i_w=1}^{N_w} \mathcal{B}_{i_w}}, \tag{40}$$

$$E_{i_w}^{(i)} = E_{L,0}^{(i_w)}\big(\vec{R}_{i_w}^{(i)}\big) + \varepsilon_{L,S}^{(i_w)}\big(\vec{R}_{i_w}^{(i)}\big), \tag{41}$$

with $E_{L,0}^{(i_w)}(\vec{R}_{i_w}^{(i)})$ and $\varepsilon_{L,S}^{(i_w)}(\vec{R}_{i_w}^{(i)})$ given by

$$E_{L,0}^{(i_w)}\big(\vec{R}_{i_w}^{(i)}\big) = \int d\vec{R}' \langle \vec{R}' | \hat{H}_0 | \vec{R}_{i_w}^{(i)} \rangle \frac{\rho_T(\vec{R}')}{\rho_T\big(\vec{R}_{i_w}^{(i)}\big)}, \tag{42}$$

$$\varepsilon_{L,S}^{(i_w)}\big(\vec{R}_{i_w}^{(i)}\big) = \sum_{l=1}^{N} \frac{c_{l,i_w}^{+}(i)}{c_{l,i_w}^{+}(i) + c_{l,i_w}^{-}(i)} \epsilon_{L,S,l}^{(i_w)}\big(\vec{R}_{i_w}^{(i)}, +1\big)$$
$$+ \frac{c_{l,i_w}^{-}(i)}{c_{l,i_w}^{+}(i) + c_{l,i_w}^{-}(i)} \epsilon_{L,S,l}^{(i_w)}\big(\vec{R}_{i_w}^{(i)}, -1\big), \tag{43}$$

$$\epsilon_{L,S,l}^{(i_w)}\big(\vec{R}_{i_w}^{(i)}, s_{l,i_w}^{i}\big)$$
$$= \sum_{\vec{S}'} \int d\vec{R}' \langle \vec{R}', \vec{S}' | \hat{w}_{\mathrm{Re},l} + \hat{V}_{\Phi,l} | \vec{R}_{i_w}^{(i)}, \vec{S}_{i_w}^{(i)} \rangle \frac{\rho_T(\vec{R}')}{\rho_T\big(\vec{R}_{i_w}^{(i)}\big)}. \tag{44}$$

Here $\hat{w}_{\mathrm{Re},l}$ and $\hat{V}_{\Phi,l}$ are the contributions from particle l to the potentials $\hat{w}_{\mathrm{Re}}$ and $\hat{V}_{\Phi}$, defined in Eqs. (17) and (18), respectively. In Eq. (40) the sum is over the complete set of N_w walkers, obtained after the standard GDB process associated to the spinless part of the Hamiltonian. In this way, the expression implicitly includes the weighting of the standard branching. Equation (40) represents the generalization of Eqs. (B8) and (B11) for the mixed-branching case.

An important remark concerning the secondary branching is that $B(j+1)$ in Eq. (39) is not positive definite. However, the fraction of walkers which generate a change in sign is

tiny, and thus walkers that produce this effect can be safely discarded. To quantify that, we monitor the quantity

$$\chi = \frac{N_e}{\langle N_w \rangle N_b}, \tag{45}$$

with N_e and N_b the number of eliminated walkers and the number of iterations per block, and $\langle N_w \rangle$ the average number of walkers of the block. Our numerical results show that χ depends slightly on the value of the parameters chosen for the simulation, but it is always of the order of 10^{-3} or smaller.

IV. DISCRETE SPIN T-MOVES DMC (DTDMC)

In this section we adapt the continuous spin T-moves method of Ref. [11] to a system of discrete spins under the SOC interactions analyzed in this work. In the following, we assume the two-body interaction is spin-dependent, with (possibly) different contributions in each channel. In this method the walkers carry explicit spin variables together with the particle positions.

A. Basics of the DTDMC method

The T-moves method [11] adapted to discrete spins can be implemented as described in this section; see Appendix C for details. One starts from a standard GDB process with the branching factor [15]

$$B(\vec{R}, \vec{R}'', \vec{S}) = \exp\left\{ -\frac{\Delta\tau}{2}[E_L(\vec{R}, \vec{S}) + E_L(\vec{R}'', \vec{S})] \right\}, \tag{46}$$

with

$$E_L(\vec{R}, \vec{S}) = \sum_{\vec{S}'} \int d\vec{R}' \langle \vec{R}', \vec{S}' | \hat{H}^{\mathrm{FP}} | \vec{R}, \vec{S} \rangle \frac{\rho_T(\vec{R}', \vec{S}')}{\rho_T(\vec{R}, \vec{S})}, \tag{47}$$

and $\hat{H}^{\mathrm{FP}}$ the fixed-phase Hamiltonian of Eq. (19). Afterwards, a transition is performed following the probability

$$p(\vec{R}'', \vec{S} \to \vec{R}'\vec{S}') = \frac{P(\vec{R}'', \vec{S} \to \vec{R}'\vec{S}')}{\sum_{\vec{S}'} \int d\vec{R}' P(\vec{R}'', \vec{S} \to \vec{R}'\vec{S}')}, \tag{48}$$

$$P(\vec{R}'', \vec{S} \to \vec{R}'\vec{S}')$$
$$= \delta(\vec{R}' - \vec{R}'')\delta(\vec{S}' - \vec{S})$$
$$- \Delta\tau \langle \vec{R}', \vec{S}' | \hat{w}_{\mathrm{Re,A}}^{\mathrm{eff}} | \vec{R}'', \vec{S} \rangle \frac{\rho_T(\vec{R}', \vec{S}')}{\rho_T(\vec{R}'', \vec{S})}, \tag{49}$$

where

$$\langle \vec{R}, \vec{S} | \hat{w}_{\mathrm{Re,A}}^{\mathrm{eff}} | \vec{R}, \vec{S} \rangle = 0,$$

$$\langle \vec{R}', \vec{S}' | \hat{w}_{\mathrm{Re,A}}^{\mathrm{eff}} | \vec{R}, \vec{S} \rangle = \begin{cases} \langle \vec{R}', \vec{S}' | \hat{w}_{\mathrm{Re}} | \vec{R}, \vec{S} \rangle & \text{if } T < 0 \\ 0 & \text{if } T > 0 \end{cases}, \tag{50}$$

with

$$T = \langle \vec{R}', \vec{S}' | \hat{w}_{\mathrm{Re}} | \vec{R}, \vec{S} \rangle \frac{\rho_T(\vec{R}', \vec{S}')}{\rho_T(\vec{R}, \vec{S})}. \tag{51}$$

The T-moves method provides an upper bound to the FPA energy due to the definition of an effective Hamiltonian in order to avoid a sign problem. This effective Hamiltonian depends

both on the phase and the magnitude of the trial wave function. For this reason, the method is variational with respect to both quantities. We showcase this property in Sec. V. Furthermore,

the two-body spin-dependent interaction is treated like any other local operator in DMC, and its contribution to the local energy is

$$
V_{\text{L,2b}}(\vec{R}, \vec{S}) = \sum_{\vec{S}'} \int d\vec{R}' \langle \vec{R}', \vec{S}' | \hat{V}_{\text{2b}} | \vec{R}, \vec{S} \rangle \frac{\rho_T(\vec{R}', \vec{S}')}{\rho_T(\vec{R}, \vec{S})} = \sum_{k<l} V^{\text{2b}}_{s_k, s_l}(r_{kl}),
\tag{52}
$$

where use has been made of the fact that the operator is local, and therefore contains terms of the form $\delta(\vec{S}' - \vec{S})\delta(\vec{R} - \vec{R}')$ The two-body, spin-dependent potential is defined in Eqs. (5) and (6).

B. Application to synthetic SOC in ultracold gases

In this section we show how to apply the previous method to the SOC interactions of interest in the field of ultracold gases. We focus on the Weyl SOC, although the procedure is analogous for the Rashba and Raman potentials. We start evaluating the matrix elements of $\hat{w}_{\text{Re}}$, which are given by

$$
\begin{aligned}
\langle \vec{R}', \vec{S}' | \hat{w}_{\text{Re}} | \vec{R}, \vec{S} \rangle = \frac{\lambda \hbar}{M} \sum_{k=1}^{N} & \left[\prod_{l \neq k} \delta(\vec{r}'_l - \vec{r}_l)\delta(s'_l - s_l) \right] \left[\delta(y'_k - y_k)\delta(z'_k - z_k) \frac{d}{dx'_k} \delta(x'_k - x_k) \right. \\
& \times \langle s'_k | \hat{\sigma}_{x,k} | s_k \rangle \sin[-\phi_k(x'_k, y_k, z_k, s'_k) + \phi_k(\vec{r}_k, s_k)] + \delta(x'_k - x_k)\delta(z'_k - z_k) \frac{d}{dy'_k} \delta(y'_k - y_k) \\
& \times \langle s'_k | -i\sigma_{y,k} | s_k \rangle \cos[-\phi_k(x_k, y'_k, z_k, s'_k) + \phi_k(\vec{r}_k, s_k)] \\
& + \delta(x'_k - x_k)\delta(y'_k - y_k) \frac{d}{dz'_k} \delta(z'_k - z_k) \\
& \left. \times \langle s'_k | \sigma_{z,k} | s_k \rangle \sin[-\phi_k(x_k, y_k, z'_k, s'_k) + \phi_k(\vec{r}_k, s_k)] \right]
\end{aligned}
\tag{53}
$$

with ϕ_k the single-particle phase of Eq. (20). In this expression we have omitted the last term of Eq. (4) as it is a constant contribution that represents a shift of the total energy only. In order to construct the effective Hamiltonian, we must evaluate the matrix elements of $\hat{w}_{\text{Re}}$ to check their sign. However, given any set of coordinates $\vec{r}_k$, $\vec{r}'_k$, terms of the form $\frac{d}{dx'_k}[\delta(x'_k - x_k)]$ are in general problematic. In order to preserve the upper bound property of the effective Hamiltonian, we adopt the (apparently rude) prescription

$$
\frac{d}{d\xi'_k}[\delta(\xi'_k - \xi_k)] \sim \frac{1}{2\epsilon}[\delta(\xi'_k + \epsilon - \xi_k) - \delta(\xi'_k - \epsilon - \xi_k)]
\tag{54}
$$

with ϵ a small parameter. This is equivalent to replacing the momentum operator with

$$
\hat{p} \sim \frac{\hbar}{2i\epsilon} \left[\exp\left(i\frac{\hat{p}}{\hbar}\epsilon\right) - \exp\left(-i\frac{\hat{p}}{\hbar}\epsilon\right) \right],
\tag{55}
$$

while both expressions coincide to order ϵ. Notice that, in this form, the resulting operator is still hermitian, and for $\epsilon \to 0$, the energy is preserved. With this substitution, $\hat{w}_{\text{Re}}$ is replaced by a new operator $\hat{w}_{\text{Re},\epsilon}$, whose matrix elements are the same as in Eq. (53) with the derivatives of the deltas replaced as in Eq. (54). We can then construct the potential $\hat{w}_{\text{Re},\epsilon,\text{A}}^{\text{eff}}$ using Eqs. (50).

Notice that, by introducing the prescription in Eqs. (54) and (55), the SOC part of the propagator becomes exact up to order $O(\frac{N\Delta\tau}{2\epsilon})$. This implies that the value of ϵ must be chosen

so that

$$
1 \gg \left| \Delta\tau \sum_{\vec{S}'} \int d\vec{R}' \langle \vec{R}', \vec{S}' | \hat{w}_{\text{Re},\epsilon,\text{A}}^{\text{eff}} | \vec{R}'', \vec{S} \rangle \frac{\rho_T(\vec{R}', \vec{S}')}{\rho_T(\vec{R}'', \vec{S})} \right|,
$$

$$
\begin{aligned}
1 \gg & \left| \Delta\tau \sum_{\vec{S}'} \int d\vec{R}' \langle \vec{R}', \vec{S}' | \hat{w}_{\text{Re},\epsilon,\text{B}}^{\text{eff}} | \vec{R}'', \vec{S} \rangle \frac{\rho_T(\vec{R}', \vec{S}')}{\rho_T(\vec{R}'', \vec{S})} \right| \\
& = \left| \Delta\tau \langle \vec{R}'', \vec{S} | \hat{w}_{\text{Re},\epsilon,\text{B}}^{\text{eff}} | \vec{R}'', \vec{S} \rangle \right|,
\end{aligned}
\tag{56}
$$

with

$$
\langle \vec{R}, \vec{S} | \hat{w}_{\text{Re},\epsilon,\text{B}}^{\text{eff}} | \vec{R}, \vec{S} \rangle = \sum_{\vec{s}} \int d\vec{X} \langle \vec{R}, \vec{S} | \hat{w}_{\text{Re},\epsilon} | \vec{X}, \vec{s} \rangle \frac{\rho_T(\vec{X}, \vec{s})}{\rho_T(\vec{R}, \vec{S})},
$$

$$
\langle \vec{R}', \vec{S}' | \hat{w}_{\text{Re},\epsilon,\text{B}}^{\text{eff}} | \vec{R}, \vec{S} \rangle = 0
\tag{57}
$$

where, in the last expression, the summation and the integration are restricted to those values that satisfy the condition $T > 0$, given in Eq. (51). We have seen in our simulations that these conditions can be somewhat relaxed. In any case, the precise value of ϵ chosen for the simulations should not affect the energy contribution from the SOC part of the Hamiltonian,

$$
\begin{aligned}
& \sum_{\vec{S}'} \int d\vec{R}' \langle \vec{R}', \vec{S}' | \hat{w}_{\text{Re},\epsilon,\text{A}}^{\text{eff}} + \hat{w}_{\text{Re},\epsilon,\text{B}}^{\text{eff}} | \vec{R}, \vec{S} \rangle \frac{\rho_T(\vec{R}', \vec{S}')}{\rho_T(\vec{R}, \vec{S})} \\
& \simeq \sum_{\vec{S}'} \int d\vec{R}' \langle \vec{R}', \vec{S}' | \hat{w}_{\text{Re}} | \vec{R}, \vec{S} \rangle \frac{\rho_T(\vec{R}', \vec{S}')}{\rho_T(\vec{R}, \vec{S})}.
\end{aligned}
\tag{58}
$$

C. The DTDMC algorithm

We discuss in this section a scheme of the DTDMC algorithm to better understand its practical implementation. A walker at iteration j is described by

$$\vec{v}(j) = \left(\vec{r}_1^{(j)}, s_1^{(j)}, \ldots, \vec{r}_N^{(j)}, s_N^{(j)}\right) \qquad (59)$$

with $s_k = \pm 1$ the z component of the spin of particle k and subindexes and superindexes standing particles and iterations, respectively. The initial condition for the position and spin coordinates is generally obtained through the sampling of the trial wave function using the Metropolis algorithm.

The first step to be implemented at each iteration is a GDB process with the branching factor given by Eq. (46), which produces a spatial translation $\vec{R}^{(j)} \rightarrow \vec{R}_A^{(j)}$. After this, we need to sample the part of the propagator which depends on the effective potential $\hat{w}_{\mathrm{Re},\epsilon,\mathrm{A}}$. In this second step, a transi-

tion $(\vec{R}_A^{(j)}, \vec{S}^{(j)}) \rightarrow (\vec{R}^{(j+1)}, \vec{S}^{(j+1)})$ is performed given by the probability

$$p(\vec{R}, \vec{S} \rightarrow \vec{R}'\vec{S}') = \frac{P(\vec{R}, \vec{S} \rightarrow \vec{R}'\vec{S}')}{\sum_{\vec{S}'} \int d\vec{R}' P(\vec{R}, \vec{S} \rightarrow \vec{R}'\vec{S}')}, \qquad (60)$$

$$P(\vec{R}, \vec{S} \rightarrow \vec{R}'\vec{S}') = \delta(\vec{R}' - \vec{R})\delta(\vec{S}' - \vec{S})$$
$$- \Delta\tau \langle \vec{R}', \vec{S}' | \hat{w}_{\mathrm{Re},\epsilon,\mathrm{A}}^{\mathrm{eff}} | \vec{R}, \vec{S} \rangle \frac{\rho_T(\vec{R}', \vec{S}')}{\rho_T(\vec{R}, \vec{S})}, \qquad (61)$$

where we can identify $\vec{R} = \vec{R}_A^{(j)}$, $\vec{S} = \vec{S}^{(j)}$, $\vec{R}' = \vec{R}^{(j+1)}$ and $\vec{S}' = \vec{S}^{(j+1)}$. As an example, we explicitly report how this evolution is carried out for the Weyl SOC case. A possible transition probability is

$$P(\vec{R}, \vec{S} \rightarrow \vec{R}', \vec{S}') = \delta(\vec{R}' - \vec{R})\delta(\vec{S}' - \vec{S}) - \Delta\tau \left(\sum_{k=1}^{N} \left[\prod_{l \neq k} \delta(\vec{r}_l' - \vec{r}_l)\delta(s_l' - s_l) \right] \times \frac{\lambda\hbar}{M} \left\{ \delta(y_k' - y_k)\delta(z_k' - z_k)\frac{1}{2\epsilon}\delta(x_k' + \epsilon - x_k) \right. \right.$$

$$\times \langle s_k' | \hat{\sigma}_{x,k} | s_k \rangle \sin[-\phi_k(x_k', y_k, z_k, s_k') + \phi_k(\vec{r}_k, s_k)] - \delta(x_k' - x_k)\delta(z_k' - z_k)\frac{1}{2\epsilon}\delta(y_k' - \epsilon - y_k)$$

$$\times \langle s_k' | -i\hat{\sigma}_{y,k} | s_k \rangle \cos[-\phi_k(x_k, y_k', z_k, s_k') + \phi_k(\vec{r}_k, s_k)]$$

$$+ \delta(x_k' - x_k)\delta(y_k' - y_k)\frac{1}{2\epsilon}\left[\delta(z_k' + \epsilon - z_k) - \delta(z_k' - \epsilon - z_k)\right]$$

$$\left. \left. \times \langle s_k' | \hat{\sigma}_{z,k} | s_k \rangle \sin[-\phi_k(x_k, y_k, z_k', s_k') + \phi_k(\vec{r}_k, s_k)] \right\} \right) \frac{\rho_T(\vec{R}', \vec{S}')}{\rho_T(\vec{R}, \vec{S})}. \qquad (62)$$

Notice that the terms appearing in $P(\vec{R}, \vec{S} \rightarrow \vec{R}', \vec{S}')$ are different for each walker and each iteration. In general, one has to keep here only those terms of Eq. (53) [after the substitution of Eqs. (54) and (55)] that are strictly negative. This total transition probability is the sum of different transition probabilities $P_{t,k}^{(m)}$, so it can be written as

$$= P_{t,k}^{(0)}(\vec{R}, \vec{S} \rightarrow \vec{R}\vec{S})\delta(\vec{R}' - \vec{R})\delta(\vec{S}' - \vec{S}) + \sum_{k=1}^{N} \left[\prod_{l \neq k} \delta(\vec{r}_l' - \vec{r}_l)\delta(s_l' - s_l) \right] \left\{ \delta(y_k' - y_k)\delta(z_k' - z_k) \right.$$

$$\times \delta(x_k' + \epsilon - x_k)P_{t,k}^{(1)}(x_k, s_k \rightarrow x_k - \epsilon, -s_k)$$

$$+ \delta(x_k' - x_k)\delta(z_k' - z_k)\delta(y_k' - \epsilon - y_k)P_{t,k}^{(2)}(y_k, s_k \rightarrow y_k + \epsilon, -s_k)$$

$$+ \delta(x_k' - x_k)\delta(y_k' - y_k)\left[\delta(z_k' + \epsilon - z_k)P_{t,k}^{(3)}(z_k, s_k \rightarrow z_k - \epsilon, s_k)\right.$$

$$\left. \left. + \delta(z_k' - \epsilon - z_k)P_{t,k}^{(4)}(z_k, s_k \rightarrow z_k + \epsilon, s_k)\right]\right\}. \qquad (63)$$

The probabilities $P_{t,k}^{(m)}$ depend on the coordinates of all particles but we only make explicit the dependence on the coordinates that change under each transition for the sake of simplicity. Notice that in this example there are $4N + 1$ possible transitions. We define the cumulative distribution vector as

$$v_c(i_c) = \frac{\sum_{i=1}^{i_c} v_2(i)}{\sum_{i=1}^{4N+1} v_2(i)}, \; i_c = 1, \ldots, 4N + 1, \quad v_c(0) = 0 \qquad (64)$$

with

$$v_2 = \left(1, P_{t,1}^{(1)}, P_{t,1}^{(2)}, P_{t,1}^{(3)}, P_{t,1}^{(4)}, \ldots, P_{t,N}^{(1)}, P_{t,N}^{(2)}, P_{t,N}^{(3)}, P_{t,N}^{(4)}\right). \qquad (65)$$

Notice that $v_c(i_c) \in (0, 1] \; \forall i_c$. To sample this discrete probability distribution function we follow the standard procedure: we generate a random number $\xi \in [0, 1]$ and select the component of $v_c(i_{\mathrm{trans}})$ that verifies

$$v_c(i_{\mathrm{trans}} - 1) < \xi,$$
$$v_c(i_{\mathrm{trans}}) > \xi. \qquad (66)$$

Finally, we perform the transition associated to the quantity $v_2(i_{\text{trans}}) = v_c(i_{\text{trans}}) - v_c(i_{\text{trans}} - 1)$, i.e., if $v_2(i_{\text{trans}}) = P_{t,k}^{(2)}$, the spin of particle k flips and its coordinates are modified according to $x_k' = x_k$, $y_k' = y_k + \epsilon$, $z_k' = z_k$, while the rest of the system is left unchanged.

V. RESULTS

We report in this Section results for the energy in different systems for both the SIDMC and DTDMC methods. In Sec. V A we show the energy of a few one-body and two-body problems, while in Sec. V B we report results for the energy of a few many-body systems, both in the mean-field regime and out of it. As a check of validity of the two DMC algorithms for SOC systems, we compare the DMC estimations with energies obtained from the imaginary-time evolution of the Schrödinger equation (one and two-body cases) and the Gross-Pitaevskii equation (many-body in the dilute regime). We also comment on the technical issues mentioned in Secs. III B and IV C, mainly the elimination of walkers in SIDMC and the influence of the parameter ϵ in DTDMC, as well as the dependence of the energy estimation on the time step. In all cases, the parameters of the Hamiltonian and the trial wave function are reported in reduced units (see Sec. II A).

A. One- and two-body problems

In this section, we report DMC results for the energy corresponding to four different physical situations: a three-dimensional (3D) one-body system with Weyl SOC, a 3D one-body system with Raman SOC, and two interacting two-dimensional (2D) two-body systems with Rashba SOC, one featuring a spin-independent two-body interaction and another with a spin-dependent one. All systems are harmonically confined. We summarize our results in Table I, which includes the DMC energies obtained with both algorithms together with the imaginary time evolution (ITE) estimates, both for the fixed-phase Hamiltonian [Eq. (19)] and the fixed-phase, effective Hamiltonian of the DTDMC approach. All SIDMC energies are obtained by performing several simulations, changing the parameter $\Delta\tau$, and then extrapolating the energy to the limit $\Delta\tau \to 0$. In the Weyl and Rashba cases with DTDMC, one must carry out several calculations changing $\Delta\tau$ and ϵ and then extrapolate to the limits $\Delta\tau \to 0$, $\epsilon \to 0$, and $\frac{\Delta\tau}{\epsilon} \to 0$. We discuss below how to perform the triple limit involving $\Delta\tau$, ϵ, and $\frac{\Delta\tau}{\epsilon}$. This setup is not necessary in the Raman calculations since the SOC part of the propagator scales as $O(N\Delta\tau)$ if ϵ is sufficiently small.

The trial wave function for each Hamiltonian is important because it fixes the phase and, in all cases, reduces the

variance via importance sampling. In the problem of Raman SOC and DTDMC the trial wave function that we have used is

$$\Psi_T(\vec{r}, s) = \rho_T(\vec{r}, s)\exp[i\phi_T(\vec{r}, s)], \tag{67}$$

$$\rho_T(\vec{r}, s = +1) = \left[C_1^2 \sin^2\mu + C_2^2 \cos^2\mu \right.$$
$$\left. + 2\sin\mu\cos\mu C_1 C_2 \cos(2kx)\right]^{1/2}$$
$$\times \exp\left[-\frac{\omega}{2}(x^2 + y^2 + z^2)\right], \tag{68}$$

$$\rho_T(\vec{r}, s = -1) = \left[C_2^2 \sin^2\mu + C_1^2 \cos^2\mu \right.$$
$$\left. + 2\sin\mu\cos\mu C_1 C_2 \cos(2kx)\right]^{1/2}$$
$$\times \exp\left[-\frac{\omega}{2}(x^2 + y^2 + z^2)\right], \tag{69}$$

$$\phi_T(\vec{r}, s = +1) = \text{atan}\left[\frac{(C_1 \sin\mu - C_2 \cos\mu)\sin(kx)}{(C_1 \sin\mu + C_2 \cos\mu)\cos(kx)}\right], \tag{70}$$

$$\phi_T(\vec{r}, s = -1) = \text{atan}\left[\frac{(C_1 \cos\mu - C_2 \sin\mu)\sin(kx)}{(C_1 \cos\mu + C_2 \sin\mu)\cos(kx)}\right] \tag{71}$$

with $\mu = \frac{1}{2}\text{acos}(\frac{k}{\eta_{\text{Rm}}})$, k the reduced momentum and ω the harmonic oscillator strength. In these expressions, $\{k, C_1, C_2\}$ are taken as variational parameters. The SOC term of the trial wave function is of the same form as the one used in Ref. [8]. Since the magnitude of the trial wave function must be independent of the spin in SIDMC, we have used

$$\rho_T(\vec{r}) = \left[C_1^2 + C_2^2 + 2B_c C_1 C_2 \cos(2kx)\right]^{1/2}$$
$$\times \exp\left[-\frac{\omega}{2}(x^2 + y^2 + z^2)\right] \tag{72}$$

with B_c another variational parameter.

Concerning the Weyl model, the adopted trial wave function for DTDMC is

$$\rho_T(\vec{r}, s = +1) = \exp\left[-\frac{\omega}{2}(x^2 + y^2 + z^2)\right], \tag{73}$$

$$\rho_T(\vec{r}, s = -1) = \frac{(1 + \cos\theta_k)}{\sin\theta_k}\exp\left[-\frac{\omega}{2}(x^2 + y^2 + z^2)\right], \tag{74}$$

$$\phi_T(\vec{r}, s = +1) = \vec{k}\vec{r}, \tag{75}$$

$$\phi_T(\vec{r}, s = -1) = \vec{k}\vec{r} + \pi + \phi_k, \tag{76}$$

where θ_k and ϕ_k are the polar and azimuthal angles of the momentum vector $\vec{k}$, respectively. The adopted magnitude of

TABLE I. Results of the energy estimation (in reduced units, see Sec. II A) for the few-body systems described in Sec. V A. Results for the Raman and Weyl cases correspond to the total energy while results for the Rashba case correspond to the energy per particle.

	SIDMC	ITE FPA	DTDMC	DTDMC fixed ϵ	ITE FPA eff. H
Raman	1.368 ± 0.001	1.3667 ± 0.0005	1.368 ± 0.001		1.3679 ± 0.0005
Weyl	1.095 ± 0.002	1.0780 ± 0.0005	1.197 ± 0.002	1.190 ± 0.002	1.1887 ± 0.0005
Rashba 2-b no spin	1.064 ± 0.002	1.058 ± 0.003	1.148 ± 0.003	1.132 ± 0.002	1.133 ± 0.003
Rashba 2-b spin			1.279 ± 0.002	1.262 ± 0.002	1.258 ± 0.003

the trial wave function for the SIDMC case is

$$\rho_T(\vec{r}) = \exp\left[-\frac{\omega}{2}(x^2 + y^2 + z^2)\right]. \quad (77)$$

Finally, the trial wave function used in the DTDMC two-body Rashba simulations is

$$\Psi_T(\vec{R}, \vec{S}) = \left[\prod_{j=1}^{2} \rho_{T,1b}(\vec{r}_j, s_j)\right] \rho_{T,2b}(\vec{r}_1, \vec{r}_2)$$

$$\times \exp\left[i\sum_{j=1}^{2}\phi_T(\vec{r}_j, s_j)\right], \quad (78)$$

$$\rho_{T,1b}(\vec{r}, s=+1) = \exp\left[-\frac{\omega}{2}(x^2 + y^2)\right], \quad (79)$$

$$\rho_{T,1b}(\vec{r}, s=-1) = \exp\left[-\frac{\omega}{2}(x^2 + y^2)\right], \quad (80)$$

$$\phi_T(\vec{r}, s=+1) = \vec{k}\vec{r} - \phi_k - \frac{\pi}{2}, \quad (81)$$

$$\phi_T(\vec{r}, s=-1) = \vec{k}\vec{r} \quad (82)$$

with ϕ_k the angle of the momentum vector in polar coordinates. In this expression, $\rho_{T,2b}(\vec{r}_1, \vec{r}_2)$ is the exact solution of the two-body interacting problem at low momentum ($k_{2b} \sim 10^{-2}$) (without SOC) corresponding to the soft-sphere potential of Eq. (6), with parameters

$$\overline{V}_0 = \frac{V_0(1,1) + V_0(1,-1) + V_0(-1,1) + V_0(-1,-1)}{4}, \quad (83)$$

$$\overline{R}_0 = \frac{R_0(1,1) + R_0(1,-1) + R_0(-1,1) + R_0(-1,-1)}{4}. \quad (84)$$

This choice makes the two-body trial wave function spin-independent for simplicity. We use the same choice for the SIDMC simulations.

The time step is $\Delta\tau \sim O(10^{-3})$ in DTDMC simulations while it is $\Delta\tau \sim O(10^{-2})$ in the SIDMC ones. The average number of walkers is kept stable along the simulations, and it is fixed to a value between 2000 and 3000, depending on the case. The parameter ϵ of DTDMC is fixed as $\epsilon = 100\Delta\tau$ in the Raman calculation and as $\epsilon = 200\Delta\tau$ in the Rashba and Weyl cases. In the Weyl SIDMC calculations, the secondary branching weights $w(j)$ are accumulated along blocks of $N_b = 10$ iterations. The ratio of eliminated walkers is $\chi < 0.001$. In the Rashba cases, we have $N_b = 50$ and $\chi < 0.002$. Finally, for the Raman problem we have $N_b = 10$ and $\chi = 0$ (see Sec. III B).

The parameters used in the Raman simulations are $\eta_{Rm} = 1$, $\omega = 0.4$, $\Omega = 0.5$, $k = 0.7$, $C_1 = 0.6$, $C_2 = 0.8$, and $B_c = 0.5$. For the Weyl simulations we considered $\eta_{We} = 1$, $\omega = 0.4$, $k = 0.5$, $\theta_k = \frac{\pi}{4}$, and $\phi_k = 0.3$. Finally, the parameters for the two-body Rashba simulations in the two-body spin-independent case are $V_0 = 1.5$, $R_0 = 3.5$, $k = 0.5$, $\phi_k = 0.1$, and $\omega = 0.4$. The two-body spin-dependent Rashba case shares the same values, except for $V_0(+1, +1) = V_0(-1, -1) = 2.5$ and $V_0(+1, -1) = V_0(-1, +1) = 1.5$.

In Fig. 1 we show the energy as a function of the imaginary-time step for the two-body Rashba calculations.
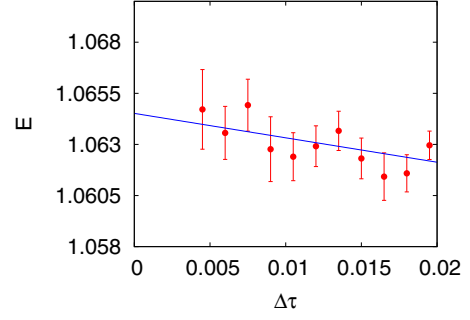

FIG. 1. Dependence of the DMC energy on the imaginary-time step using the SIDMC method for a two-body system with Rashba SOC and harmonic confinement. The line corresponds to the linear extrapolation of the DMC energies. Quantities are dimensionless, with the energy and length scales defined in Eq. (8).

We can clearly see a linear dependence of the energy with the time step, as it corresponds to a linear approximation to the exact propagator. In the DTDMC method, as stated previously, three limits have to be satisfied in order to obtain the estimation of the energy: $\Delta\tau \to 0$, $\epsilon \to 0$, and $\frac{\Delta\tau}{\epsilon} \to 0$. The extrapolations according to these limits can be performed in several ways. Here we present two of them. Method 1 consists on performing N_{sets} sets of N_{sim} simulations making $\Delta\tau \to 0$, $\epsilon \to 0$, with $\frac{\Delta\tau}{\epsilon} \ll 1$ fixed. After this, one ends up with N_{sets} estimations of the energy, each one associated to a given $\frac{\Delta\tau}{\epsilon}$ value. Finally, one retains the estimation associated to the lowest $\frac{\Delta\tau}{\epsilon}$ value. Method 2 consists in performing N_{sets} sets of N_{sim} simulations making $\Delta\tau \to 0$, $\frac{\Delta\tau}{\epsilon} \to 0$, with ϵ fixed. After this, one ends up with N_{sets} estimations of the energy, each one associated to a given ϵ value. Finally, one then takes the extrapolation of these estimations in the limit $\epsilon \to 0$.

In Figs. 2 and 3 we show the estimations obtained using Method 1 and Method 2, respectively, for the one-body system with Weyl SOC and a harmonic trap. As we can see, the dependence of the energy extrapolations with respect to $\frac{\Delta\tau}{\epsilon}$ is much weaker than their dependence on ϵ. Therefore, Method 1 is preferred and is the one that we have used to provide the T-moves energy. We can also see from the figure that the
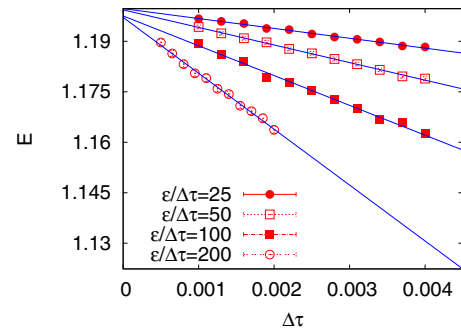

FIG. 2. Estimation of the DTDMC energy using Method 1 for a one-body system with Weyl SOC and a harmonic trap. The lines correspond to the linear extrapolation of the DMC energies. Quantities are dimensionless, with the energy and length scales defined in Eq. (10).
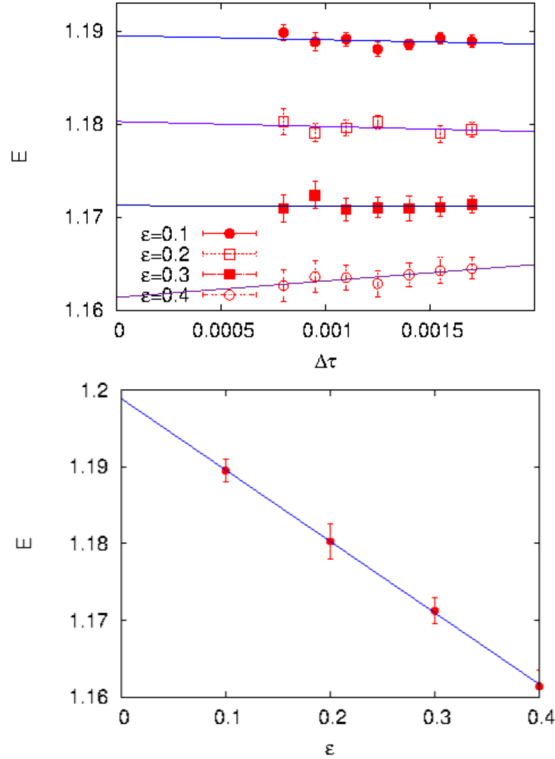
FIG. 3. Estimation of the DTDMC energy using Method 2 for a one-body system with Weyl SOC and a harmonic trap. The lines correspond to the linear extrapolation of the DMC energies. The quantities shown are dimensionless.

dependence of the energy with respect to $\Delta\tau$, when ϵ or $\frac{\Delta\tau}{\epsilon}$ are fixed, is linear in both cases. This is because the non-SOC terms of the propagator are exact up to $O(\Delta\tau)$ while the SOC terms are exact up to $O(\frac{\Delta\tau}{\epsilon})$. For all the chosen values of ϵ, the conditions in Eq. (56) are satisfied, with the r.h.s being 10^{-2}. Also, the condition in Eq. (58) is satisfied since the difference between the r.h.s. and the l.h.s. is at most a 3% of the SOC local energy contribution.

From Table I, we can see that both DMC methods provide energies that agree with the result of the imaginary-time evolution within a 2% error. We can also see that SIDMC provides lower energies than DTDMC. This is due to the fixed-phase nature of the energies obtained with SIDMC, which does not require to use an effective Hamiltonian as DTDMC. We can see that this effect is enhanced in the harmonically trapped systems featuring Rashba and Weyl SOCs. For the cases with two-body spin-dependent interactions, only T-moves results are reported, since SIDMC can not deal with these kind of potentials. It must be remarked that, while in the T-moves calculations we perform the triple extrapolation $\Delta\tau \to 0$, $\epsilon \to 0$, and $\frac{\Delta\tau}{\epsilon} \to 0$, calculations with ITE are performed at a fixed ϵ ($\epsilon = 0.1$ and $\epsilon = 0.3$ in the Weyl and Rashba cases, respectively). This is due to the computational cost of decreasing ϵ when discretizing the Schrödinger equation in the position representation, since ϵ is taken as the point-to-point distance of the mesh. In order to check that both DTDMC and ITE give compatible estimates, we also provide in Table I DMC energies corresponding to a fixed ϵ. This is not necessary in the Raman case since the Raman Hamiltonian

is independent of ϵ if this parameter is sufficiently small, as mentioned previously. Notice also that the errors corresponding to the ITE results in the two-body 2D Rashba cases are larger than the ones in the 3D one-body Raman and Weyl cases. This is due to the higher number of dimensions that must be discretized in the latter case.

B. Many-body calculations

We report in this section the DMC energies corresponding to the many-body Raman and Weyl SOC Hamiltonians. We first focus on the dilute regime with a finite number of particles imposing periodic boundary conditions (PBCs). We compare the DMC energy estimations with energies obtained by solving the imaginary time Gross-Pitaevskii equation (GPE), both for the fixed-phase Hamiltonian [Eq. (19)] and the fixed-phase, effective Hamiltonian of the DTDMC approach. In the case of Rashba SOC, we do not know the scattering length of the complete interaction, and thus a direct comparison to GPE is not possible. Finally, we compare the energy estimations of both DMC methods out of the dilute regime.

1. Dilute regime

Table II reports the DMC energy per particle together with the corresponding Gross-Pitaevskii energy per particle, for four different physical systems: Raman SOC and Weyl SOC, both with spin-independent and spin-dependent two-body interactions. Moreover, we include the T-moves energy per particle using two different trial wave functions in the two-body spin-independent Weyl case in order to showcase the variational dependence of this method with respect to the magnitude of the trial wave function.

For the GPE calculations involving Raman or Weyl SOCs, we use the free-space scattering length, i.e., the scattering length obtained for the Hamiltonian removing the SOC terms [19,20].

In all cases, the trial wave function is of the form

$$\Psi_T(\vec{R}, \vec{S}) = \left[\prod_{j=1}^{N} \rho_{T,\mathrm{1b}}(\vec{r}_j, s_j) \right] \prod_{\substack{i,j=1 \\ i<j}}^{N} \overline{\rho}_{T,\mathrm{2b}}(\vec{r}_i, \vec{r}_j)$$

$$\times \exp\left[i \sum_{j=1}^{2} \phi_T(\vec{r}_j, s_j) \right], \quad (85)$$

with

$$\overline{\rho}_{T,\mathrm{2b}}(r_{ij}) = \begin{cases} \dfrac{\rho_{T,\mathrm{2b}}(r_{ij}) + \rho_{T,\mathrm{2b}}(L - r_{ij})}{2\rho_{T,\mathrm{2b}}(L/2)} & \text{if } r_{ij} < L/2 \\ 1 & \text{if } r_{ij} > L/2 \end{cases} \quad (86)$$

and $r_{ij} = |\vec{r}_i - \vec{r}_j|$. The function $\rho_{T,\mathrm{2b}}(r_{ij})$ is the magnitude of a spin-independent two-body trial wave function analogous to the one presented in Sec. V A (here $k_{\mathrm{2b}} \sim 10^{-6}$). The magnitude of the one-body terms for the T-moves "Raman 2-b no spin" and "Raman 2-b spin" cases are given in Eqs. (68) and (69). For the SIDMC "Raman 2-b no spin" case we use the expression in Eq. (72). Both DTDMC and SIDMC "Weyl 2-b no spin" cases are done with the terms in Eq. (77), while in the T-moves "Weyl 2-b no spin trial 2" and "Weyl 2-b spin" cases we use the one-body forms of Eqs. (73) and (74). In

TABLE II. Results of the energy per particle (in reduced units, see Sec. II A) for the many-body systems in the dilute regime, as described in Sec. V B 1.

	SIDMC	GPE FPA	DTDMC	DTDMC fixed ϵ	GPE FPA eff. H
Raman 2-b no spin	-0.0496 ± 0.0002	-0.04964 ± 0.00005	-0.0496 ± 0.0004		-0.04962 ± 0.00005
Raman 2-b spin			0.00946 ± 0.00004		0.009370 ± 0.000005
Weyl 2-b no spin	0.1125 ± 0.0003	0.11217 ± 0.00005	0.1444 ± 0.0002	0.1423 ± 0.0002	0.14239 ± 0.00005
Weyl 2-b no spin trial 2			0.1122 ± 0.00015	0.1123 ± 0.00015	0.11225 ± 0.000005
Weyl 2-b spin			0.0602 ± 0.0001	0.0602 ± 0.0001	0.06029 ± 0.00005

all cases no harmonic trap has been used. The trial phases for each case are analogous to the ones in Eqs. (70), (71), (75), and (76).

The average number of walkers is set to $N_w = 1000$ and the time step is $\Delta\tau \sim O(10^{-3})$. The parameter ϵ of DTDMC is fixed as $\epsilon = 100\Delta\tau$. All the used values of ϵ satisfy the condition of Eq. (58), with a discrepancy between the r.h.s. and the l.h.s. of at most $\sim 1\%$. Also, the r.h.s of both expressions in Eq. (56) equals 0.08 at most, which implies that the maximum error in the approximation to the propagator is $e_{\max} \sim e^{0.08} - (1 + 0.08) \simeq 0.0033$. In the Weyl SIDMC calculations, the length of a simulation block is set to $N_b = 10$. The ratio of eliminated walkers is $\chi < 0.0002$. For the Raman calculations, we have $N_b = 10$ and $\chi = 0$ (see Sec. III B).

The Raman simulations are carried out with $N = 40$ particles, $\eta_{\text{Rm}} = 0.4$, $L_x = L_y = L_z = 16.899$ (box length) and $k = k_x = \frac{2\pi}{L_x}$. In the two-body spin-independent case we have $V_0 = 75$, $R_0 = 0.25$, $\Omega = 0.4$, $C_1 = 0$, $C_2 = 1$ and $B_c = 0.5$, while in the two-body spin-dependent case we have $V_0(+1, +1) = V_0(-1, -1) = 75$, $V_0(+1, -1) = V_0(-1, +1) = 50$, $R_0 = 0.25$, $\Omega = 0.1$, $C_1 = 0.6$, $C_2 = 0.8$. The gas parameter for these systems is $na^3 \simeq 10^{-6}$.

In the Weyl simulations, and for the two-body spin-independent case, we use $N = 45$ particles, $\eta_{\text{We}} = 0.25$, $L_x = L_y = L_z = 20$, $\vec{k} = (k_x, 0, k_z)$ with $k_i = \frac{2\pi}{L_i}$, $V_0 = 75$, $R_0 = 0.3$, with a gas parameter of $na^3 = 1.7 \times 10^{-5}$. In the two-body spin-dependent case we use $N = 35$, $\eta_{\text{We}} = 0.25$, $L_x = L_y = L_z = 18$, $k = k_x = \frac{2\pi}{L_x}$, $V_0(+1, +1) = V_0(-1, -1) = 75$, $V_0(+1, -1) = V_0(-1, +1) = 50$, $R_0 = 0.3$, with a gas parameter of $na^3 \sim 10^{-5}$.

We can see from Table II that the DMC energies agree with the GPE calculations up to a $\sim 1\%$. As in the previous section, for the spin-dependent two-body cases only T-moves results are reported, since the SIDMC method can not solve two-body spin-dependent interactions. We can also see from the two-body spin-independent cases that DTDMC is able to recover almost completely the fixed-phase energy, although we know it always provides an upper bound to it. On the other hand, SIDMC recovers the complete fixed-phase energy. The DTDMC Weyl two-body spin-independent calculations illustrate the variational property with respect to the magnitude of the trial wave function of this method. Notice that two different magnitudes ("Weyl 2-b no spin" and "Weyl 2-b no spin" cases) provide two different energy estimations.

2. Beyond the dilute regime

In this section we compare the performance of the two DMC algorithms discussed in several homogeneous many-

body systems, beyond the dilute regime. We analyze a few systems featuring Raman and Weyl SOCs using periodic boundary conditions, and a two-body spin-independent interaction. We show again an example of the variation of the T-moves energy when the magnitude of the trial wave function is changed. We also provide DTDMC energy estimations of systems under Raman and Weyl SOCs with a spin-dependent two-body interaction. Finally, we compare both DMC estimations in a many-body harmonically confined system with Weyl SOC. Results are presented in Table III.

The general form of the trial wave function is given in Eq. (85). The T-moves calculations corresponding to the cases "Raman PBC 2-b no spin," "Raman PBC 2-b spin trial 1," and "Raman PBC 2-b spin trial 2" use the one-body terms of Eqs. (68) and (69), while for the SIDMC "Raman PBC 2-b no spin" calculation Eq. (72) has been used. For DTDMC corresponding to the cases "Weyl PBC 2-b no spin," "Weyl PBC 2-b spin," and "Weyl HO 2-b no spin" we use the expressions in Eqs. (73) and (74) while for the DTDMC "Weyl PBC 2-b no spin trial 2" case we use

$$\rho_T(\vec{r}, s = +1) = \gamma, \tag{87}$$

$$\rho_T(\vec{r}, s = -1) = \sqrt{1 - \gamma^2} \frac{(1 + \cos\theta_k)}{\sin\theta_k}, \tag{88}$$

$$\gamma = 0.6. \tag{89}$$

This form helps us to illustrate the variational property of the T-moves method with respect to the magnitude of the trial wave function. The SIDMC "Weyl PBC 2-b no spin" and "Weyl HO 2-b no spin" calculations use the expressions in Eq. (77). As in the previous section, the trial phases for each case are given in Eqs. (70), (71), (75), and (76).

In the two-body spin-independent calculations, the two-body trial terms in all PBC cases are the same as in Sec. V B 1.

TABLE III. Energies (in reduced units, see Sec. II A) for the many-body systems out of the dilute regime, as described in Sec. V B 2.

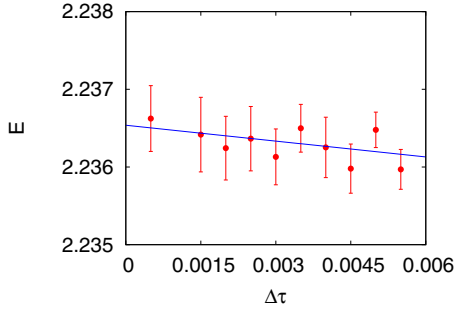|	SIDMC	DTDMC
Raman PBC 2-b no spin	3.673 ± 0.002	3.681 ± 0.002
Raman PBC 2-b spin trial 1		5.356 ± 0.003
Raman PBC 2-b spin trial 2		5.358 ± 0.002
Weyl PBC 2-b no spin	3.773 ± 0.003	3.798 ± 0.003
Weyl PBC 2-b no spin trial 2		4.050 ± 0.005
Weyl PBC 2-b spin		5.633 ± 0.005
Weyl HO 2-b no spin	2.236 ± 0.001	2.302 ± 0.002

FIG. 4. Dependence of the DMC energy on the imaginary time step for SIDMC for a many-body system with Weyl SOC and a harmonic trap. The line corresponds to the linear extrapolation of the DMC energies. The shown quantities are dimensionless.

Concerning the two-body spin-dependent calculations, we report the energy in the Weyl case using a spin-independent two-body correlation factor analogous to the one in Sec. V B 1. In the Raman case, though, we compare the energy estimated using a spin-independent two-body factor with that estimated using a spin-dependent one, again with the same form as in Sec. V B 1. Finally, in the "Weyl HO 2-body no spin" case we set $\overline{\rho}_{T,2b}(r_{ij}) = \rho_{T,2b}(r_{ij})$ in Eq. (86) because we do not impose PBC.

The average number of walkers is set to $N_w = 1000$, the time step $\Delta\tau \in (10^{-4}, 10^{-3})$, and the DTDMC ϵ parameter is fixed such that $\frac{\epsilon}{\Delta\tau} \in (100, 400)$ for Weyl and $\frac{\epsilon}{\Delta\tau} = 10$ for Raman. All the used values of ϵ satisfy the condition in Eq. (58), with a discrepancy between the r.h.s. and the l.h.s. of at most 3%. Also, the r.h.s of both expressions in Eq. (56) equals 0.3 at most, which implies that the maximum error in the approximation to the propagator is $e_{max} \sim e^{0.3} - (1 + 0.3) \simeq 0.05$. In the Weyl PBC SIDMC calculations the length of a simulation block is set to $N_b = 10$. The ratio of eliminated walkers is $\chi < 0.006$. The harmonically trapped Weyl simulations share the same parameters except for the ratio of eliminated walkers, $\chi < 0.001$. For the Raman calculations one has $N_b = 10$ and $\chi = 0$ (see Sec. III B).

In the Raman case we use $N = 50$ particles, $\eta_{Rm} = 1.5$, $\Omega = 0.4$, $L_x = L_y = L_z = 4.5$, $V_0 = 1$, $R_0 = 1.5$, $k = \frac{2\pi}{L_x}$, and $C_1 = 0.6$, $C_2 = 0.8$. In the SIDMC simulations we also
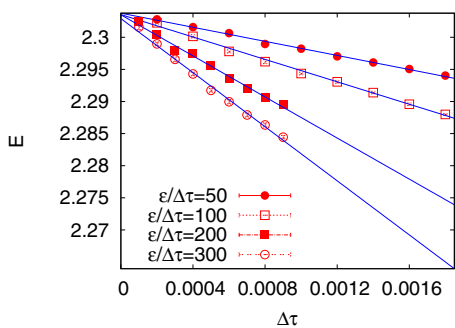

FIG. 5. Estimation of the DTDMC energy using Method 1 for a many-body system with Weyl SOC and a harmonic trap. The lines correspond to the linear extrapolation of the DMC energies. The shown quantities are dimensionless.
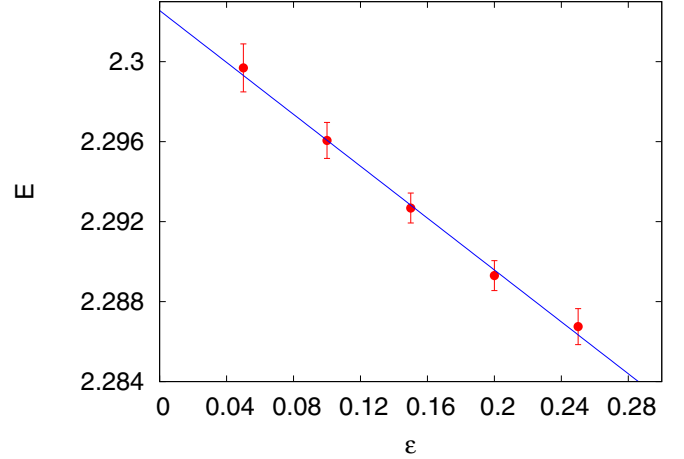

FIG. 6. Estimation of the DTDMC energy using Method 2 for a many-body system with Weyl SOC and a harmonic trap. The line corresponds to the linear extrapolation of the DMC energies. All quantities are dimensionless.

have $B_c = 0.5$. The two-body spin-dependent case shares the same parameters with the exception of $V_0(+1, +1) = V_0(-1, -1) = 2$, $V_0(+1, -1) = V_0(-1, +1) = 1$. The gas parameter for the up-down channels is $na^3 \sim 10^{-2}$ while for the up-up and down-down channels we set $na^3 \sim 0.1$. In the PBC two-body spin-independent Weyl case we simulate $N = 25$ particles with $\eta_{We} = 3.590$, $L_x = L_y = L_z = 3.5$, $V_0 = 1$, $R_0 = 1.5$, and $\vec{k} = (k_x, 0, 0)$ $k_x = \frac{2\pi}{L_x}$. The two-body spin-dependent case shares the same parameters with the exception of $V_0(+1, +1) = V_0(-1, -1) = 2$, $V_0(+1, -1) = V_0(-1, +1) = 1$. The gas parameter for each channel is of the same order of magnitude that the one in the Raman case. Finally, in the harmonically trapped Weyl simulations we use $N = 30$ particles, $\eta_{We} = 1$, $\omega = 0.4$, $V_0 = 1$, $R_0 = 1.5$, $k = 0.5$, $\theta_k = 1.31$, and $\phi_k = 0.3$.

In Fig. 4 we show the energy dependence on the imaginary time step corresponding to the SIDMC simulations of trapped Weyl gases. We can see in the figure the linear dependence of the energy with respect to $\Delta\tau$. In Figs. 5 and 6 we show DTDMC results for the two methods mentioned in Sec. V A to estimate the triple limit $\Delta\tau \to 0$, $\epsilon \to 0$, and $\frac{\Delta\tau}{\epsilon} \to 0$. The observed behavior is consistent with the previous results obtained in the one-body case.

In Table III we report the DMC energies for the analyzed cases. From these results, we can see that DTDMC is able to almost exactly recover the fixed-phase energy of the bulk gases. In the trapped Weyl gas, the difference with respect to the fixed-phase energy obtained with SIDMC is larger. We can also see how the improvement of the magnitude of the trial wave function in the two-body spin-independent PBC Weyl simulation produces better energies as a consequence of the variational property of the DTDMC method. Finally, our results show that the spin-dependent two-body trial correlation factor does not make any significant difference in the two-body spin-dependent PBC Raman simulation.

VI. CONCLUSIONS

In this paper, we discuss two different diffusion Monte Carlo methods (DTDMC and SIDMC) that are able to deal with many-body systems of ultracold quantum gases featuring synthetic spin-orbit coupling. DTDMC is an extended version of the method of Refs. [11] and [15] to the relevant SOC interactions in the field of ultracold gases, but with discrete spins. This method relies on the introduction of an effective Hamiltonian and provides an upper bound to the fixed-phase energy of the system. On the contrary, the SIDMC method is able to avoid this issue by propagating the spin-integrated probability density, providing exact fixed-phase estimations. However, SIDMC is not able to deal with spin-dependent two-body interactions and requires the use of spin-independent trial wave functions.

We have described the formalism of both methods in detail, together with a scheme of both algorithms for future applications. We have reported the energy estimation of several few-body systems, featuring three different kinds of SOC interactions. We have compared these results with energies obtained by propagating the Schrödinger equation in imaginary time, finding good agreement between both estimations. We have also performed simulations of many-body systems in the dilute regime and have recovered the energies obtained by solving the imaginary time Gross-Pitaevskii equation with discrepancies of at most ∼1%. Finally, we have compared both algorithms beyond the dilute regime, showing that the DTDMC method is able to recover the fixed-phase energy almost completely in the PBC cases. We hope that these methods can be used to explore the physics of SOC systems beyond the mean field, dilute regime.

ACKNOWLEDGMENTS

APPENDIX A: THE SPIN-ORBIT PROPAGATOR IN THE FIXED-PHASE APPROXIMATION

In this appendix we derive a suitable form of the propagator required to simulate spin-orbit problems, under the assumption that the two-body interaction $\hat{V}^{2b}$ is spin-independent. The imaginary time evolution of state $|\Psi(\tau)\rangle$ is given by

$$|\Psi(\tau + \Delta\tau)\rangle = \exp[-\Delta\tau \hat{H}]|\Psi(\tau)\rangle. \tag{A1}$$

Projecting on $\langle \vec{R}', \vec{S}'|$ and introducing an identity, Eq. (A1) can be written as

$$\psi(\vec{R}', \vec{S}', \tau + \Delta\tau) = \sum_{\vec{S}} \int d\vec{R} \langle \vec{R}', \vec{S}'| \exp[-\Delta\tau \hat{H}]|\vec{R}, \vec{S}\rangle \\ \times \psi(\vec{R}, \vec{S}, \tau), \tag{A2}$$

where $\vec{R}$ and $\vec{S}$ stand for the position and spin coordinates of the N particles and $\psi(\vec{R}, \vec{S}, \tau) = \langle \vec{R}, \vec{S}||\Psi(\tau)\rangle$. For the sake of clarity, we also define

$$\hat{H}_0 = \sum_{k=1}^{N}\left[\frac{P_k^2}{2M} + \hat{V}_k^{1b} + \sum_{l<k}^{N}\hat{V}_{k,l}^{2b}\right], \tag{A3}$$

$$\hat{W} = \sum_{k=1}^{N}\hat{W}_k^{\text{SOC}}. \tag{A4}$$

Up to $O(\Delta\tau)$, Eq. (A2) can be written as

$$\psi(\vec{R}', \vec{S}', \tau + \Delta\tau) \\ = \sum_{\vec{S}}\int d\vec{R}\int d\vec{R}''\langle \vec{R}', \vec{S}'|\exp[-\Delta\tau\hat{W}]|\vec{R}'', \vec{S}\rangle \\ \times \langle \vec{R}''|\exp[-\Delta\tau\hat{H}_0]|\vec{R}\rangle\psi(\vec{R}, \vec{S}, \tau) + O(\Delta\tau^2), \tag{A5}$$

where the term corresponding to $\hat{H}_0$ in the splitting of $\hat{H}$ in the propagator is spin-independent.

In this way, the propagator reads

$$G(\vec{R}, \vec{S} \to \vec{R}', \vec{S}') = \int d\vec{R}''\langle \vec{R}', \vec{S}'|\exp[-\Delta\tau\hat{W}]|\vec{R}'', \vec{S}\rangle \\ \times \langle \vec{R}''|\exp[-\Delta\tau\hat{H}_0]|\vec{R}\rangle. \tag{A6}$$

This propagator can have complex contributions coming from the Pauli matrices appearing in the spin-orbit interaction, and therefore sampling it is not possible. In order to bypass this problem, we resort to the fixed-phase approximation [11] where all quantities involved are real.

Knowing the general expression of the propagator written above, we can deduce its reduction to the fixed-phase approximation. This can be done comparing the imaginary-time Schrödinger equation for the wave function and for its magnitude, which is the main quantity of interest in the FPA. For the full wave function, one has

$$-\frac{\partial\psi(\vec{R}, \vec{S})}{\partial\tau} = \left\{\sum_{k=1}^{N}\left[-\frac{\hbar^2}{2M}\nabla_k^2 + V_k^{1b}(\vec{r}_k) + \sum_{l<k}^{N}\hat{V}_{k,l}^{2b}(r_{kl})\right]\right\} \\ \times \psi(\vec{R}, \vec{S}, \tau) \\ + \sum_{\vec{S}'}\int d\vec{R}'\langle \vec{R}, \vec{S}|\hat{W}|\vec{R}', \vec{S}'\rangle\psi(\vec{R}', \vec{S}', \tau), \tag{A7}$$

while for the magnitude $\rho(\vec{R}, \vec{S})$ of $\psi(\vec{R}, \vec{S})$ the equation reads

$$-\frac{\partial\rho(\vec{R}, \vec{S})}{\partial\tau} = \left\{\sum_{k=1}^{N}\left[-\frac{\hbar^2}{2M}\nabla_k^2 + \frac{\hbar^2}{2M}\left|\vec{\nabla}_k\Phi(\vec{R}, \vec{S}, \tau)\right|^2 \\ + V_k^{1b}(\vec{r}_k) + \sum_{l<k}^{N}\hat{V}_{k,l}^{2b}(\vec{r}_k, \vec{r}_l)\right]\right\}\rho(\vec{R}, \vec{S}, \tau) \\ + \sum_{\vec{S}'}\int d\vec{R}'\langle \vec{R}, \vec{S}|\hat{w}_{\text{Re}}|\vec{R}', \vec{S}'\rangle\rho(\vec{R}', \vec{S}', \tau), \tag{A8}$$

where

$$\psi(\vec{R}, \vec{S}, \tau) = \rho(\vec{R}, \vec{S}, \tau) \exp[i\Phi(\vec{R}, \vec{S}, \tau)] \quad \text{(A9)}$$

and

$$\langle \vec{R}, \vec{S}|\hat{w}_{\text{Re}}|\vec{R}', \vec{S}'\rangle = \text{Re}\left\{ \langle \vec{R}, \vec{S}|\hat{W}|\vec{R}', \vec{S}'\rangle \frac{e^{i\Phi(\vec{R}', \vec{S}', \tau)}}{e^{i\Phi(\vec{R}, \vec{S}, \tau)}} \right\}. \quad \text{(A10)}$$

In the FPA, $\Phi(\vec{R}, \vec{S}, \tau)$ is independent of τ and $\hat{V}_\Phi = \sum_{k=1}^N |\nabla_k \Phi(\vec{R}, \vec{S}, \tau)|^2$ becomes a local interaction in positions and spins. Equations (A7) and (A8) have a similar structure, and thus comparing terms in each, we can get the FPA form of the propagator in Eq. (A6):

$$G_{\text{FP}}(\vec{R}, \vec{S} \to \vec{R}', \vec{S}')$$
$$= \langle \vec{R}', \vec{S}'| \exp[-\Delta\tau \hat{H}^{\text{FP}}]|\vec{R}, \vec{S}\rangle$$
$$= \int d\vec{R}'' \langle \vec{R}', \vec{S}'| \exp\left[-\Delta\tau\left(\hat{w}_{\text{Re}} + \hat{V}_\Phi\right)\right]|\vec{R}'', \vec{S}\rangle$$
$$\times \langle \vec{R}''| \exp[-\Delta\tau \hat{H}_0]|\vec{R}\rangle + O(\Delta\tau^2), \quad \text{(A11)}$$

with

$$\hat{H}^{\text{FP}} = \hat{H}_0 + \hat{w}_{\text{Re}} + \hat{V}_\Phi \quad \text{(A12)}$$

the fixed-phase Hamiltonian.

APPENDIX B: ENERGY ESTIMATION IN THE SIDMC METHOD

We show in this appendix how to estimate the energy of a many-body system under SOC interactions using the method presented in Sec. III, although it can be easily extended to estimate any other quantity. The DMC energy estimator in the FPA at iteration j is given by

$$E_{\text{DMC}}(j) = \sum_{\vec{S}, \vec{S}'} \int d\vec{R}^{(j)} d\vec{R}' \langle \vec{R}', \vec{S}'|\hat{H}^{\text{FP}}|\vec{R}^{(j)}, \vec{S}\rangle$$
$$\times \frac{\rho_T(\vec{R}')}{\rho_T(\vec{R}^{(j)})} f(\vec{R}^{(j)}, \vec{S}, j\Delta\tau), \quad \text{(B1)}$$

with $\hat{H}^{\text{FP}}$ defined in Eq. (19). The local energy is, therefore,

$$E_L = \sum_{\vec{S}'} \int d\vec{R}' \langle \vec{R}', \vec{S}'|\hat{H}^{\text{FP}}|\vec{R}^{(j)}, \vec{S}\rangle \frac{\rho_T(\vec{R}')}{\rho_T(\vec{R}^{(j)})}, \quad \text{(B2)}$$

which, as it can be seen, depends on $\vec{R}^{(j)}$ and $\vec{S}$, so that $E_L = E_L(\vec{R}^{(j)}, \vec{S})$. We can split it in two parts

$$E_L(\vec{R}^{(j)}, \vec{S}) = E_{L,0}(\vec{R}^{(j)}) + E_{L,S}(\vec{R}^{(j)}, \vec{S}), \quad \text{(B3)}$$

corresponding the the spin-independent and spin-dependent contributions, respectively. The spin-independent part can be expressed in the form

$$E_{L,0}(\vec{R}^{(j)}) = \int d\vec{R}' \langle \vec{R}'|\hat{H}_0|\vec{R}^{(j)}\rangle \frac{\rho_T(\vec{R}')}{\rho_T(\vec{R}^{(j)})}, \quad \text{(B4)}$$

while

$$E_{L,S} = \sum_{\vec{S}'} \int d\vec{R}' \langle \vec{R}', \vec{S}'|\hat{w}_{\text{Re}} + \hat{V}_\Phi|\vec{R}^{(j)}, \vec{S}\rangle \frac{\rho_T(\vec{R}')}{\rho_T(\vec{R}^{(j)})}$$
$$= \sum_{l=1}^N \epsilon_{L,S,l}(\vec{R}^{(j)}, s_l), \quad \text{(B5)}$$

with $\epsilon_{L,S,l}$ the one-body contribution to the spin-dependent local energy corresponding to particle l (recall that $\hat{w}_{\text{Re}} + \hat{V}_\Phi$ is a one-body operator). With all these definitions, Eq. (B1) becomes

$$E_{\text{DMC}}(j) = E_{\text{DMC},0}(j) + E_{\text{DMC},S}(j). \quad \text{(B6)}$$

The term $E_{\text{DMC},0}(j)$ contains all the spin-independent contributions, and can be written as

$$E_{\text{DMC},0}(j) = \int d\vec{R}^{(j)} E_{L,0}(\vec{R}^{(j)}) \sum_{\vec{S}} f(\vec{R}^{(j)}, \vec{S}, j\Delta\tau)$$
$$= \int d\vec{R}^{(j)} E_{L,0}(\vec{R}^{(j)}) F(\vec{R}^{(j)}, j\Delta\tau) \quad \text{(B7)}$$

with $F(\vec{R}, \tau)$ defined in Eq. (29). This part of the energy is evaluated as usual in DMC, i.e.,

$$E_{\text{DMC},0}(j) = \frac{1}{N_w} \sum_{i_w=1}^{N_w} E_{L,0}^{(i_w)}(\vec{R}^{(j)}), \quad \text{(B8)}$$

where N_w is the total number of walkers in the simulation, and i_w specifies the walker index. In much the same way

$$E_{\text{DMC},S}(j) = \sum_{l=1}^N \sum_{s_l=\pm 1} \int d\vec{R}^{(j)} \epsilon_{L,S,l}(\vec{R}^{(j)}, s_l)$$
$$\times \tilde{F}(\vec{R}^{(j)}, s_l, j\Delta\tau) \quad \text{(B9)}$$

with

$$\tilde{F}(\vec{R}^{(j)}, s_l, j\Delta\tau) = \text{eval} \sum_{\vec{S}_{N-l}} f(\vec{R}^{(j)}, \vec{S}, j\Delta\tau)|_{s_k=\pm 1}, \quad \text{(B10)}$$

where $\sum_{\vec{S}_{N-1}}$ in the second term means summing over the spins of all particles but the kth one. Therefore, we need to be able to sample $\tilde{F}(\vec{R}^{(j)}, s_l, j\Delta\tau)$ in order to evaluate $E_{\text{DMC},S}(j)$. This can be done by estimating $E_{\text{DMC},S}(j)$ as

$$E_{\text{DMC},S}(j) = \frac{1}{N_w}\left[\sum_{i_w=1}^{N_w} \sum_{l=1}^N \frac{c_{l,i_w}^+(j)}{c_{l,i_w}^+(j) + c_{l,i_w}^-(j)} \epsilon_{L,S,l}^{(i_w)}(\vec{R}^{(j)}, +1) \right.$$
$$\left. + \frac{c_{l,i_w}^-(j)}{c_{l,i_w}^+(j) + c_{l,i_w}^-(j)} \epsilon_{L,S,l}^{(i_w)}(\vec{R}^{(j)}, -1) \right]$$
$$= \frac{1}{N_w} \sum_{i_w=1}^{N_w} \varepsilon_{L,S}^{(i_w)}(\vec{R}^{(j)}). \quad \text{(B11)}$$

This expression ensures that each local energy contribution $\epsilon_{L,S,l}^{(i_w)}(\vec{R}^{(j)}, \pm 1)$ is averaged with an effective weight given by

$$\eta_l^\pm(j) = \frac{c_l^\pm(j)}{c_l^+(j) + c_l^-(j)} w(j). \quad \text{(B12)}$$

It can be shown that this is the weight associated to the sampling of $\tilde{F}(\vec{R}^{(j)}, s_l = \pm 1, j\Delta\tau)$.

APPENDIX C: DERIVATION OF THE DTDMC ALGORITHM

In order to derive the DTDMC algorithm, one has to go back to the beginning and work out the propagator in Eq. (14),

which we split in a different way rearranging terms as

$$
\begin{aligned}
G_{\text{FP}}&(\vec{R}, \vec{S} \rightarrow \vec{R}', \vec{S}') \\
&= \int d\vec{R}'' \langle \vec{R}', \vec{S}'| \exp[-\Delta\tau \hat{w}_{\text{Re}}]|\vec{R}'', \vec{S}\rangle \\
&\quad \times \langle \vec{R}'', \vec{S}| \exp[-\Delta\tau \hat{H}_1]|\vec{R}, \vec{S}\rangle + O(\Delta\tau^2), \quad \text{(C1)}
\end{aligned}
$$

where

$$
\hat{H}_1 = \sum_{k=1}^{N} \left[\frac{P_k^2}{2M} + \hat{V}_k^{\text{1b}} + |\vec{\nabla}_k \Phi_T(\vec{R}, \vec{S})|^2 \right] + \hat{V}^{\text{2b}}. \quad \text{(C2)}
$$

We can introduce the importance sampling function inside this expression and write

$$
\begin{aligned}
\frac{\rho_T(\vec{R}', \vec{S}')}{\rho_T(\vec{R}, \vec{S})} & G_{\text{FP}}(\vec{R}, \vec{S} \rightarrow \vec{R}', \vec{S}') \\
&= \int d\vec{R}'' \frac{\rho_T(\vec{R}', \vec{S}')}{\rho_T(\vec{R}'', \vec{S})} \langle \vec{R}', \vec{S}'| \exp[-\Delta\tau \hat{w}_{\text{Re}}]|\vec{R}'', \vec{S}\rangle \\
&\quad \times \frac{\rho_T(\vec{R}'', \vec{S})}{\rho_T(\vec{R}, \vec{S})} \langle \vec{R}'', \vec{S}| \exp[-\Delta\tau \hat{H}_1]|\vec{R}, \vec{S}\rangle + O(\Delta\tau^2).
\end{aligned}
$$
(C3)

To order $O(\Delta\tau)$, the first term inside the integral becomes

$$
\begin{aligned}
\frac{\rho_T(\vec{R}', \vec{S}')}{\rho_T(\vec{R}'', \vec{S})} & \langle \vec{R}', \vec{S}'| \exp[-\Delta\tau \hat{w}_{\text{Re}}]|\vec{R}'', \vec{S}\rangle \\
&\simeq \delta(\vec{R}' - \vec{R}'')\delta(\vec{S}' - \vec{S}) \\
&\quad - \Delta\tau \langle \vec{R}', \vec{S}'| \hat{w}_{\text{Re}}|\vec{R}'', \vec{S}\rangle \frac{\rho_T(\vec{R}', \vec{S}')}{\rho_T(\vec{R}'', \vec{S})}. \quad \text{(C4)}
\end{aligned}
$$

However, for any kind of spin-orbit coupling the matrix element $\langle \vec{R}', \vec{S}'| \hat{w}_{\text{Re}}|\vec{R}'', \vec{S}\rangle$ is not always negative, and thus Eq. (C4) can not be interpreted as a probability distribution. In order to bypass this limitation and in the spirit of Refs. [11,15,16], we define an effective Hamiltonian that replaces the original one, and that leads to a variational upper bound to the fixed phase energy of the original Hamiltonian. We thus write

$$
\hat{H}_{\text{eff}}^{\text{FP}} = \hat{H}_1 + \hat{w}_{\text{Re,A}}^{\text{eff}} + \hat{w}_{\text{Re,B}}^{\text{eff}}, \quad \text{(C5)}
$$

where the sum $\hat{w}_{\text{Re,A}}^{\text{eff}} + \hat{w}_{\text{Re,B}}^{\text{eff}}$ is an approximation to the original $\hat{w}_{\text{Re}}$ of Eq. (17). This approximation is built such that the local energy of $\hat{H}_{\text{eff}}^{\text{FP}}$ and $\hat{H}^{\text{FP}}$ are equal when they act on the magnitude of the trail wave function. The matrix elements of these terms are given by

$$
\langle \vec{R}, \vec{S}| \hat{w}_{\text{Re,A}}^{\text{eff}}|\vec{R}, \vec{S}\rangle = 0,
$$
$$
\langle \vec{R}', \vec{S}'| \hat{w}_{\text{Re,A}}^{\text{eff}}|\vec{R}, \vec{S}\rangle = \begin{cases} \langle \vec{R}', \vec{S}'| \hat{w}_{\text{Re}}|\vec{R}, \vec{S}\rangle & \text{if } T < 0 \\ 0 & \text{if } T > 0 \end{cases}
$$
(C6)

with the transition coefficients

$$
T = \langle \vec{R}', \vec{S}'| \hat{w}_{\text{Re}}|\vec{R}, \vec{S}\rangle \frac{\rho_T(\vec{R}', \vec{S}')}{\rho_T(\vec{R}, \vec{S})}, \quad \text{(C7)}
$$

while

$$
\langle \vec{R}, \vec{S}| \hat{w}_{\text{Re,B}}^{\text{eff}}|\vec{R}, \vec{S}\rangle = \sum_{\vec{s}} \int dX \langle \vec{R}, \vec{S}| \hat{w}_{\text{Re}}|\vec{X}, \vec{s}\rangle \frac{\rho_T(\vec{X}, \vec{s})}{\rho_T(\vec{R}, \vec{S})},
$$
$$
\langle \vec{R}', \vec{S}'| \hat{w}_{\text{Re,B}}^{\text{eff}}|\vec{R}, \vec{S}\rangle = 0, \quad \text{(C8)}
$$

where in the last expression, the summation and the integration are restricted to those values that satisfy the condition $T > 0$. Using these definitions we avoid nonlocal matrix elements producing negative transition probabilities. Notice also that the effective Hamiltonian depends on the magnitude of the trial wave function, which means that the the energy obtained depends on its choice. The fixed-phase propagator for the effective Hamiltonian, with importance sampling, is thus

$$
\begin{aligned}
\frac{\rho_T(\vec{R}', \vec{S}')}{\rho_T(\vec{R}, \vec{S})} & G_{\text{FP}}^{\text{eff}}(\vec{R}, \vec{S} \rightarrow \vec{R}', \vec{S}') \\
&= \int d\vec{R}'' \frac{\rho_T(\vec{R}', \vec{S}')}{\rho_T(\vec{R}'', \vec{S})} \langle \vec{R}', \vec{S}'| \exp[-\Delta\tau \hat{w}_{\text{Re,A}}^{\text{eff}}]|\vec{R}'', \vec{S}\rangle \\
&\quad \times \frac{\rho_T(\vec{R}'', \vec{S})}{\rho_T(\vec{R}, \vec{S})} \langle \vec{R}'', \vec{S}| \exp[-\Delta\tau (\hat{H}_1 + \hat{w}_{\text{Re,B}}^{\text{eff}})]|\vec{R}, \vec{S}\rangle \\
&\quad + O(\Delta\tau^2). \quad \text{(C9)}
\end{aligned}
$$

Since this propagator is positive-definite, we can now interpret it as a probability distribution. Therefore, one can sample from it. This can be implemented performing initially a GDB of the $\exp[-\Delta\tau (\hat{H}_1 + \hat{w}_{\text{Re,B}}^{\text{eff}})]$ part, with a branching factor that, according to Ref. [15], reads

$$
B(\vec{R}, \vec{R}'', \vec{S}) = \exp \left\{ -\frac{\Delta\tau}{2}[E_L(\vec{R}, \vec{S}) + E_L(\vec{R}'', \vec{S})] \right\}
$$
(C10)

with

$$
E_L(\vec{R}, \vec{S}) = \sum_{\vec{S}'} \int d\vec{R}' \langle \vec{R}', \vec{S}'| \hat{H}_{\text{eff}}^{\text{FP}}|\vec{R}, \vec{S}\rangle \frac{\rho_T(\vec{R}', \vec{S}')}{\rho_T(\vec{R}, \vec{S})},
$$
(C11)

which generates the displacement $\vec{R} \rightarrow \vec{R}''$. In a second step, one performs a transition $(\vec{R}'', \vec{S}) \rightarrow (\vec{R}', \vec{S}')$ given by the probability

$$
p(\vec{R}'', \vec{S} \rightarrow \vec{R}'\vec{S}') = \frac{P(\vec{R}'', \vec{S} \rightarrow \vec{R}'\vec{S}')}{\sum_{\vec{S}'} \int d\vec{R}' P(\vec{R}'', \vec{S} \rightarrow \vec{R}'\vec{S}')}, \quad \text{(C12)}
$$

where

$$
P(\vec{R}'', \vec{S} \rightarrow \vec{R}'\vec{S}') = \delta(\vec{R}' - \vec{R}'')\delta(\vec{S}' - \vec{S}) - \Delta\tau \langle \vec{R}', \vec{S}'| \hat{w}_{\text{Re,A}}^{\text{eff}}|\vec{R}'', \vec{S}\rangle \frac{\rho_T(\vec{R}', \vec{S}')}{\rho_T(\vec{R}'', \vec{S})}. \quad \text{(C13)}
$$

Despite the sum in Eq. (C12) involves the 2^N spin configurations, which sounds prohibitive for large N, it must be kept in mind that only one-body operators are involved and the expression is greatly simplified.

[1] F. Wilczek, Nat. Phys. **5**, 614 (2009).

[2] J. D. Koralek, C. P. Weber, J. Orenstein, B. A. Bernevig, S.-C. Zhang, S. Mack, and D. D. Awschalom, Nature (London) **458**, 610 (2009).

[3] M. Z. Hasan and C. L. Kane, Rev. Mod. Phys. **82**, 3045 (2010).

[4] Y. J. Lin, K. Jiménez-García, and I. B. Spielman, Nature (London) **471**, 83 (2011).

[5] J. Dalibard, F. Gerbier, G. Juzeliūnas, and P. Öhberg, Rev. Mod. Phys. **83**, 1523 (2011).

[6] N. Goldman, G. Juzeliūnas, P. Öhberg, and I. B. Spielman, Rep. Prog. Phys. **77**, 126401 (2014).

[7] L. Zhang and X.-J. Liu, *Synthetic Spin-Orbit Coupling in Cold Atoms* (World Scientific, Singapore, 2013), pp. 1–87.

[8] Y. Li, G. I. Martone, and S. Stringari, *Annual Review of Cold Atoms and Molecules* (World Scientific, Singapore, 2015), p. 201–250.

[9] Y. Li, L. P. Pitaevskii, and S. Stringari, Phys. Rev. Lett. **108**, 225301 (2012).

[10] J. Li, J. Lee, W. Huang, S. Burchesky, B. Shteynas, F. Ç. Top, A. O. Jamison, and W. Ketterle Nature (London) **543**, 91 (2017).

[11] C. A. Melton, M. C. Bennett, and L. Mitas, J. Chem. Phys. **144**, 244113 (2016).

[12] C. A. Melton, M. Zhu, S. Guo, A. Ambrosetti, F. Pederiva, and L. Mitas, Phys. Rev. A **93**, 042502 (2016).

[13] A. Ambrosetti, F. Pederiva, and E. Lipparini, Phys. Rev. B **83**, 155301 (2011).

[14] A. Ambrosetti, P. L. Silvestrelli, F. Pederiva, L. Mitas, and F. Toigo, Phys. Rev. A **91**, 053622 (2015).

[15] M. Casula, S. Moroni, C. Filippi, and S. Sorella, J. Chem. Phys. **132**, 154113 (2010).

[16] D. F. B. ten Haaf, H. J. M. van Bemmel, J. M. J. van Leeuwen, W. van Saarloos, and D. M. Ceperley, Phys. Rev. B **51**, 13039 (1995).

[17] A. Ambrosetti, F. Pederiva, E. Lipparini, and S. Gandolfi, Phys. Rev. B **80**, 125306 (2009).

[18] R. Guardiola, Monte Carlo techniques in the many-body problem, in *First International Course on Condensed Matter*, ACIF Series, Vol. 8, edited by D. Prosperi *et al.* (World Scientific, Singapore, 1988), pp. 156–229.

[19] X. Cui, Phys. Rev. A **85**, 022705 (2012).

[20] P. Zhang, L. Zhang, and Y. Deng, Phys. Rev. A **86**, 053608 (2012).